INVESTIGATING THE ROLE OF CEREBELLAR PURKINJE CELLS IN CONTROL OF THE TONGUE IN MARMOSETS

by

Nikhil Dave

A thesis submitted to Johns Hopkins University in conformity with the requirements for the degree of Master of Science in Engineering

Baltimore, Maryland

May 2021

Abstract

The common marmoset (*Callithrix jacchus*) is a promising non-human primate model for studying cerebellar contributions to motor control. Critical in many of the marmoset's behaviors, marmosets use their specialized tongue to feed and even send visual cues to potential mates. The objective of this analysis is to elucidate the characteristics of marmoset licking behavior within the framework of our experimental setup and to provide a characterization of marmoset cerebellar Purkinje neuron responses to licking behavior at both a cellular and population level. Recording cerebellar Purkinje cells (P-cells) in awake marmoset subjects completing saccade related tasks, tongue movements were recorded using a video camera and tracked. In total, 63 Purkinje cells were recorded from lobule VI of the marmoset cerebellum and analyzed. Analysis was done on Purkinje cells identified as tongue related through visual and auditory feedback during recording. The simple spike firing rates of these cells were compared to tongue behavior quantified through tracking. It was observed that P-cells differ in their simple spike modulation from a baseline firing rate in response to the onset of licking bouts. Rhythmically firing P-cells were observed to differ in their phasic relationship to rhythmic licking.

Thesis Readers

Dr. Reza Shadmehr, PhD (Principal Investigator)
Professor
Department of Biomedical Engineering
Johns Hopkins University

Dr. Joshua Vogelstein, PhD
Assistant Professor
Department of Biomedical Engineering
Johns Hopkins University

Dr. Kechen Zhang, PhD
Associate Professor
Department of Biomedical Engineering
Johns Hopkins University

Acknowledgements

The work reported in this paper was supported by grants from the National Science Foundation (CNS-1714623), the NIH (R01-EB028156, R01-NS078311), and the Office of Naval Research (N00014-15-1-2312).

This work would not be possible without the contributions of lab members at the Laboratory for Computational Motor Control at Johns Hopkins School of Medicine. A tremendous amount of work was done by members of the Laboratory for Computational Motor Control in caring for the marmoset subjects used in this analysis. Members of the lab were responsible for creation of the experimental setup. Paul Hage, Ehsan Sedaghat-Nejad, and Jay Pi were all responsible for the electrophysiological recording of the marmoset subjects. Paul Hage, Jay PI, Ehsan Sedaghat-Nejad, and Dr. Reza Shadmehr sorted the Purkinje cell data in preparation for analysis. In Kyu Jang was responsible for enabling the 3-D markerless pose estimation used to quantify marmoset lick movements. Vivian Looi was responsible for ensuring the quality of the markerless tracking. Without all of their contributions, this work would not be possible.

I would like to acknowledge the leadership and mentorship of Paul Hage throughout development of this work. Paul Hage's coordination of a team effort to tackle the investigation of marmoset licking behavior was integral in making this work possible. His guidance and mentorship were essential for the formation of this thesis. Paul, it was a joy to work with you throughout my time at the lab. Thank you for helping me become a better engineer and scientist.

I would also like to thank Dr. Reza Shadmehr for this mentorship throughout my time as a master's student in the lab. His willingness to work with and mentor new students despite roadblocks posed by

the COVID-19 pandemic was sincerely appreciated. Dr. Shadmehr's guidance was instrumental in the formation of this thesis.

Finally, I would like to acknowledge Ehsan Sedaghat-Nejad for his help in creating the analytical framework used in this analysis.

Dedication

This thesis is dedicated to my mother, father, and sister for their love and support.

Contents

List of Figures

Chapter 1. Introduction

1.1 Lingual Anatomy

1.1.1 Musculature (Kim & Naqvi, 2020)

Lingual anatomy is characterized by its complex musculature involving intrinsic and extrinsic muscles.

The four extrinsic muscles are the genioglossus, hyoglossus, styloglossus, and the palatoglossal. The genioglossus is responsible for drawing the tongue forward from the root of the tongue. The hyoglossus muscle is used to retract the tongue and depress its sides. The styloglossus muscle's role is to draw the tongue upward. The palatoglossal muscle is responsible for raising the posterior region of the tongue (Rathee & Jain, 2020).

The four intrinsic muscles are the superior and inferior longitudinales, verticalis, and the transversus (Lin & Barkhaus, 2009). These muscles function to change the shape of the tongue by shortening, curving, and narrowing its shape (Lin & Barkhaus, 2009).

1.1.2 Innervation (Kim & Naqvi, 2020)

The tongue musculature is innervated by the efferent hypoglossal nerve. The hypoglossal nerve originates from the lower medulla in the brainstem and migrates down to the tongue. It is also referred to as the 12th cranial nerve (CN XII) and is primarily a motor, somatic nerve. This nerve innervates all the intrinsic and extrinsic muscles with exception to the palatoglossal muscle of the tongue. The palatoglossal muscle is motor innervated by the vagal nerve (CN X).

1.1.3 Behavioral Coordination

The tongue's multiple functions in different behaviors such as chewing, swallowing, speech, and breathing typically involves coordination and coupling between multiple neural systems and musculature. Along with tongue involvement, chewing requires the coordination of face and jaw muscles. Similarly, swallowing involves coordination with the pharynx and speech with the larynx. Even more complex, breathing involves synchrony of respiratory muscles in the diaphragm, abdomen, neck, and ribs.

1.2 Feeding Behavior

1.2.1 Appetitive and Consummatory Stages (Travers et al., 1997)

When describing feeding behavior, it can be generally defined as having appetitive and consummatory stages. Appetitive movements, in regard to their motor function, are both highly adaptable and diverse. In contrast consummatory movements are highly stereotyped, if not completely reflexive. While fundamental movements, like licking, are generally invariant, they are still receptive to stimuli like accessibility (Marowitz & Halpern, 1973), taste (Davis & Smith, 1992), and aversive stimuli (Wiesenfeld et al., 1977). The latter is capable of suspending licking behavior after it is initiated, however, downstream movements like swallowing are typically reflexive and will continue to completion once initiated (Wiesenfeld et al., 1977).

1.2.2 Feeding Electromyography (EMG) Studies (Travers et al., 1997)

Electromyography studies examining feeding behavior have elucidated the adaptability of licking in rat animal models (Travers & Norgren, 1986). Researchers have recorded EMG data from four different oro-pharyngeal muscles, specifically the genioglossus, anterior digastric, styloglossus, and pharyngeal

constrictor muscles responsible for tongue protrusion, jaw opening, tongue retraction, and swallowing respectively, in two experimental conditions (Travers & Norgren, 1986). In the first case, the recordings correspond to behavior in which animals licked from a water bottle (Travers & Norgren, 1986). In the second case, animals were delivered food via intra-oral cannula forcing them to lick intra-orally (Travers & Norgren, 1986). Comparing the data from both cases, the experimenters concluded that there appears to be a common masticatory-lingual motor pattern typified by a tongue protrusion and jaw opening phase followed by a tongue retraction and jaw closing phase (Hiiemae & Crompton, 1985). The timing this motor pattern appears to differ according to specific behavioral demands and illustrates the adaptability of licking as a mechanism for retrieval and intra-oral transport (Halpern, 1977).

1.3 Temporal Sequence of the Consummatory Response and Spatial Mapping in the Brainstem (Travers et al., 1997)

The temporal sequence of the consummatory response is as follows peri-oral (jaw opening), licking, and swallowing. In this order these movements are characterized as being the most flexible and adaptable to being the most reflexive, with jaw opening being the most adaptable and swallowing being the most reflexive. Additionally, each of these behaviors are possibly spatially organized in the brainstem to some degree. Peri-oral function involves the most rostral sites and also involves the anterior medullary and pontine circuits. Licking function involves circuits immediately caudal to the ones corresponding to jaw opening function and relies on complex multisynaptic RF pathways. Caudal to the circuits corresponding to peri-oral function are those required for the generation of swallowing behavior. These medullary circuits have some overlap with those for licking. Additionally, swallowing involves direct projections from NST neurons to esophageal motoneurons in the nucleus ambiguous (Cunningham & Sawchenko, 1989). These NST neurons receive input from the superior laryngeal nerve (Cunningham & Sawchenko, 1989).

1.4 Rhythmic Oromotor Movement

1.4.1 Types of Movements

When describing movements three categories are used: reflexive, voluntary, and rhythmic (Bryant, 2010). Reflexive movements are defined as being the simplest type of movement and are involuntary in nature (Hooper, 2001). These types of movements can be described as stereotyped and require a sensory input to illicit a response. Such sensory inputs require no threshold to be surpassed but must have a stimulus large enough to activate the relevant sensory pathway (Hooper, 2001). Corresponding to their distinction as the simplest type of movement, reflexive movements do not require higher brain centers to take place (Bryant, 2010). In contrast, voluntary movements are goal-driven and are characterized by directed movements like reaching for example (Hooper, 2001). These movements are more complex and are not stereotypical or repetitive (Hooper, 2001). As opposed to reflexive movements, voluntary movements can be improved through learning and repetition (Bryant, 2010). Rhythmic movements incorporate aspects of both reflexive and voluntary movements making them an interesting point of study (Bryant, 2010). Uniquely, they are considered to be complex in contrast to reflexive movements and both repetitive and stereotyped in contrast to voluntary movements (Hooper, 2001). Rhythmic motor patterns typically involve the activation of either the brainstem or spinal cord and can be initiated by external, goal-oriented stimulus (Bryant, 2010).

1.4.2 Rhythmic Oromotor Behavior

Rhythmic oromotor behavior is comprised of a number of different related movements as exemplified by the ingestion process (Hooper, 2001). The motor patterns associated with this process are characterized by a distinct sequence of movements coordinating a variety of anatomical structures including but not limited to the tongue and jaw (Travers et al., 1997). Looking closely at the

consumption of food, regardless of the type of food (solid versus liquid), the expression of common motor patterns is conserved (Hiiemae & Crompton, 1985; Threxton, 1992; Travers et al., 1997; Zeigler, 1991). While mastication involves the strategic repositioning of food during chewing and the corresponding continuous sensory monitoring, consumption of liquid foods via licking is relatively simple (Travers et al., 1997). With that said, rhythmic licking still involves the coordination of jaw opening, tongue protrusion, tongue retraction, and jaw closing (Bryant, 2010). This behavior is strongly stereotyped and appears to be conserved across numerous mammalian species (Bryant, 2010).

1.5 Central Pattern Generators (CPG) Contribution to Rhythmic Movement

1.5.1 Central Pattern Generators (CPGs)

Central pattern generators, or CPGs, are neural networks that produce rhythmic outputs without the presence of rhythmic inputs, regardless of their sensory or central origin (Hooper, 2001). The rhythmically patterned outputs of these neural networks regulate the generation of most rhythmic motor patterns (Hooper, 2001). CPGs have been a popular subject of study and their behavior has made them excellent models for understanding neural network function (Hooper, 2001). CPGs have been found to produce repetitive, periodic neural firing that can stabilize motorneuron firing, in studies related to rhythmic oromotor behavior patterns (Bryant, 2010; Nistri et al., 2006).

1.5.2 Rhythmic Licking and CPGs

Searching for the origin of rhythmic motor patterns, the first evidence for the proposition that they may be centrally generated came from experiments involving the locust nervous system (Hooper, 2001). It was observed that the nervous system of the locust would produce similar rhythmic output when

isolated from the animal as it would during flight (Hooper, 2001; Wilson, 1961 cited in Marder and Calabrese, 1996).

Due to the nature of rhythmic licking as a strongly stereotyped behavior and motor pattern, it is natural to pursue the discovery of its potential connection to CPGs and whether they could be potentially organizing such rhythmic motor patterns (Travers et al., 1997). Studies involving rat models have demonstrated evidence that 6-8 Hz modal frequency licking is controlled by a central timing mechanism that is to some extant immune to interruptions or disruptions (Travers et al., 1997). Studies involving experiments in which a rat's rhythmic licking is interrupted have shown evidence to suggest that such interferences do not reset rhythm generators (Hernandez-Mesa et al. 1988; Travers et al., 1997). In particular, these experiments have provided indications of central rhythmic activity in periods of time between licking (Hernandez-Mesa et al. 1988; Travers et al., 1997). In these experiments researchers observed the presence of electric field potentials in the proximity of the hypoglossal nucleus (mXII) in the periods between licking (Hernandez-Mesa et al. 1988; Travers et al., 1997). Similar to that of the early locust experiment other studies have also observed central hypoglossal activity in the absence of visible licking, suggesting the preservation of central rhythmic activity despite the lack of visible licks (Wiesenfeld et al., 1977; Travers et al., 1997).

Currently, the physiological properties and identity of the neurons and networks that make up CPGs are not anatomically well defined. However, it is known that rhythmic tongue movements are driven by the hypoglossal nuclei in the medulla. Looking closer at CPGs, motor programs seem to exist among premotor neural networks that transmit rhythmic inputs to collections of motor neurons that innervate the cranial nerve nuclei V, VII, and XII (Bryant, 2010; Nakamura & Katakura, 1995; Travers et al., 1997). There is also evidence to suggest that among premotor neurons in the medullary reticular formation (RF), a substrate for rhythmic licking is organized (Bryant, 2010). These neurons are encompassed within a larger, complex network of interconnected nuclei within the medullary and pontine reticular

formation (RF) that drive greater oromotor function. For example, the premotor neurons of extrinsic and intrinsic tongue muscle groups have been located within numerous medullary and pontine RF cell groups (Bryant, 2010; Kandel et al., 2000b cited in Bryant, 2010; Travers & Rinaman, 2002). In particular to rhythmic licking, rhythmically active neurons have been found in the parvocellular and intermediate zones of the RF (Bryant, 2010; Travers et al., 1997).

1.6 Cerebellum's Contribution to Oromotor Movements

1.6.1 Rat Cerebellectomy and Inactivation Studies

Studies focused on understanding the role of the cerebellum in fluid licking have investigated how the temporary or permanent loss of cerebellar function effects rhythmic licking behavior (Bryant et al., 2010). Functional rat ablation studies have resulted in a considerable reduction in lick frequency consistent with studies that involved permanent removal of the rat cerebellum as well as the temporary block of cerebellar spike output, illustrating commonality across different mammalian species (Bryant et al., 2010; Vajnerová et al., 2000). In studies involving mice animal models, the partial, short-term inactivation of cerebellar output through muscimol injections into the cerebellar nuclei resulted in a substantial slowing of lick rhythm compared to pre-treatment behavior and saline control (Bryant et al., 2010). The same study also examined the lick rhythm of cerebellectomized mice models and found a similar slowing of lick rhythm. They also noted a reduction in lick efficiency reflected by a decrease of fluid intake measured in volume per lick in both cerebellectomized and muscimol groups (Bryant et al., 2010).

1.6.2 Guinea Pig Ablation Studies (Byrd & Luschei, 1980)

Studies examining the mastication cycle of guinea pigs (*Cavia porcellus*) before and after gross ablation of the cerebellum noted that the rodents' behavior was extremely ataxic exemplified by a lack of

balance during locomotion. However, mastication was distinctly not impaired. The experimenters found that mastication cycle duration time increased while the variability of mastication cycle duration time decreased after ablation. It was also noted that the complex bilateral chew cycle of the guinea pigs was conserved post-ablation.

1.6.3 Cerebellum and Oromotor Movement

These studies go on to suggest that the cerebellum is involved, at some capacity, in the coordination of licking temporally (Bryant et al., 2010). Critical movements like licking, breathing, and swallowing have been shown to be controlled by central pattern generators (CPGs) (Barlow, 2009; Bryant et al., 2010; Cifra et al., 2009; Nistri et al., 2006). It is possible that cerebellar coordination of CPGs has an anatomical substrate, based on evidence of cerebellar nuclei projections into the brainstem corresponding to areas associated with licking, breathing, and swallowing CPGs (Asanuma et al., 1983; Bryant et al., 2010; Teune et al., 2000). In mice with their deep cerebellar nuclei and cerebellar peduncles removed, a slowing of lick rhythm was observed indicating that the cerebellum is not necessary for the generation of tongue and general oromotor movements (Bryant et al., 2010).

1.7 Spatial Representation of Lingual System in Primate Cerebellum

1.7.1 Non-Human Primate Stimulation Electromyography (EMG) Studies (Aldes & Bowman, 1979)

Researchers have investigated the representation of the tongue within the cerebellar nuclei of old-world rhesus macaques (*Macaca mulatta*) using electrophysiologic techniques. The experiments involved stimulating cerebellar nuclei while simultaneously recording the electromyography of tongue musculature, both externally and internally through needle electrodes. Analysis of the experimental

EMG results revealed that the tongue is represented in all four deep cerebellar nuclei (DCN). However, it was noted that this representation was not equivalent in each DCN.

1.8 Dysfunctional Cerebellum Effect on Oromotor Control

Dysfunction of the cerebellum can hinder lingual and general oromotor control. Two specific medical conditions that exemplify this include dysarthria and dysphagia. Dysarthria being a motor speech disorder and dysphagia being a disorder characterized by a difficulty swallowing.

1.8.1 Dysarthria (Motor Speech Disorder)

It is known that cerebellar lesions of any kind can be the cause of dysarthria (Amarenco & Hauw 1990; Gordon, 1996). To take a closer look at the relationship between cerebellar disease in humans, researchers have investigated areas of cerebellar damage associated with dysarthria (Lechtenberg & Gilman, 1978). Cerebellar lesions like vascular malformation, tumors, abscesses, hemorrhages, and infarctions were all found to be linked to dysarthria (Lechtenberg & Gilman, 1978). Examining clinical, surgical, and autopsy data, these investigators noted that there was no correlation between the degree of cerebellar vermal damage and the development of disordered speech (Lechtenberg & Gilman, 1978). However, dysarthria was found to occur in the aftermath of resections into the cerebellum extending into the paravermal region, particularly that of the left hemisphere (Lechtenberg & Gilman, 1978). Other studies have also called attention to this region, noting that cerebellar lesions that involve the paravermal rostral zone are particularly associated with dysarthria (Amarenco & Hauw 1990; Gordon, 1996).

1.8.2 Dysphagia (Swallowing Disorder) (Rangarathnam, 2014)

While it is often taken for granted, swallowing is a complex process involving salivation, sensory processing, both voluntary and reflexive motor control, as well as other processes (Zald & Pardo, 1999). Hence it follows that swallowing involves oromotor anatomy and contributions from numerous systems including both cortical and subcortical structures. Dysphagia is characterized by an impairment of the motor aspects of swallowing and more specifically by abnormal bolus flow (Robbins et al., 1999) Bolus refers to food that has been chewed and rounded, ready for swallowing. In trying to understand the connection between the cerebellum and dysphagia, investigations relating cerebellar lesions with dysphagia have yielded inconclusive results. Examining results across many human subject studies, dysphagia is present in subjects with cerebellar lesions, but not to such a severe degree as in individuals with wide-spread lesions. While it is important to note that cerebellar lesions could be the cause of dysphasia, there are discrepancies within literature.

1.9 Marmoset Model

1.9.1 Geography (Downey, 2017)

The common marmoset *Callithrix jacchus,* is a promising non-human primate model for studying cerebellar contributions to motor control. A new world monkey, the common marmoset's original habitat was comprised of the northeastern coast of Brazil in the country's Atlantic coastal forests, however, human pressure on these ecosystems and increasing habitat destruction in the region has forced these animals to seek new environments throughout Brazil. The common marmoset is known for being able to adjust and flourish in new environments which other animals may find to be inhospitable. The species has been seen in dry secondary forests, riverine forests, and savanna forests, attesting to its

highly adaptable nature. It is important to note that common marmosets are most commonly found at the edge of these habitats as opposed to their center.

1.9.2 Characteristics and Lifespan (Downey, 2017)

The common marmoset is a small monkey species with characteristically long tails. Males tend to exceed females in size with a male-to-female body mass ratio of ~0.964 (Smithsonian). The average body length for males is roughly 19 cm and that of females is 18.5 cm. The average body weight of males is 256 g versus females' 236 g. The monkey's characteristically long tail can add another ~30cm of length to the animal. As an animal model, the common marmoset has been of interest to scientists due to its short gestation period of just ~5 months, propensity to give birth to non-identical twins or triplets, and biological adaptation to give seasonal births typically resulting in two pregnancies a year. This high breeding efficiency indicates potential for germline transmission of genetically modified models. A defining feature of the species, common marmosets exhibit social behavior and exist in family units. One such social behavior is cooperative infant care in which fathers, older siblings, and even extended family will contribute to a child's care.

1.9.3 Contribution of Tongue Control in Critical Behaviors (Downey, 2017)

Stemming from their nature as a social species, the common marmoset utilizes a collection of vocalization patterns to communicate information. Vocalizations include but are not limited to the alarm calls, trill calls, and phee calls. Alarm calls can be vocalized in two forms, but the purpose is the same: to warn other members of the group of a potential danger. They can either be sequence of repeated calls of increasing tone or a series of abbreviated, gradually appearing calls that can be either intermittent or continuous. Trill calls are low in pitch and are characterized by a vibrato sound that fluctuates in frequency. These calls are used by all members of the group regardless of their gender or age and are

used by the monkeys to keep track of each other's whereabouts, especially in low visibility areas. Phee calls are high pitched whistles consisting of a series of one to five notes lasting typically two seconds each and are sounded by marmosets in defending territory, attracting a potential mate, locating a lost member, and in support group cohesion.

The common marmoset is not limited to vocalization as a method of communicating to other members of its species. While vocalization is a tool marmosets utilize when communicating over long distances, they can use visual cues to share information with each other at close range. Many of these visual signals involve the oromotor system. A partial open mouth stare can be a signal for alarm and a frown can be a sign of aggression. Interestingly, female marmosets will flick their tongue in a distinctive manner to solicit potential male partners.

The diet of the common marmoset consists primarily of exudates and insects. Making up 70% of the marmoset diet, plant exudates are the secretions of plants like sap, resin, and gum. The monkeys are uniquely adapted to this obtaining this food source. Using their claws as anchors to cling to the sides of trees, they will prompt the flow of the exudates by using their teeth to gnaw a hole into the trees. Using their specialized tongue, they will then lick their food for nourishment.

1.9.4 The Marmoset Brain (Fujita et al., 2010)

The marmoset cerebellar cortex demonstrates organization by transverse foliation and longitudinal compartmentalization. The folial and compartmental organization of the marmoset cerebellum resembles that of the macaque cerebellum. The outer shapes and major fissures of the cerebella of both animals appear to be very similar, however, it is important to note that they differ in size. The marmoset cerebellum is smaller in size and is roughly half the length of the macaque cerebellum. Additionally, the vermis of the marmoset tends to be wider and the hemisphere smaller than that of a macaque. Researchers have examined molecular compartmentalization as a tool to understand the organization of

the mammalian cerebellum. In particular, it has been shown that cerebellar expression of aldolase C and its corresponding compartmentalization may be used to understand the fundamental functional organization of the cerebellar cortex. Studies comparing the compartmental organization of aldolase C in marmosets and rodents reinforces the notion that the marmoset cerebellum reflects the common, phylo-genetically preserved fundamental organization of the mammalian cerebellum.

1.10 Specific Aims

The first specific aim of this analysis is to elucidate the characteristics of marmoset licking behavior within the framework of our experimental setup. The second objective of this paper is to provide a characterization of marmoset cerebellar Purkinje neuron responses to licking behavior at both a cellular and population level.

Chapter 2. Materials and Methods

2.1 Experimental Setup (Sedaghat-Nejad et al., 2019)

A detailed description of the experimental setup used to acquire the data analyzed in this paper is described in the following paper: *Behavioral training of marmosets and electrophysiological recording from the cerebellum* (Sedaghat-Nejad et al., 2019). To summarize the experimental setup, the following description is provided.

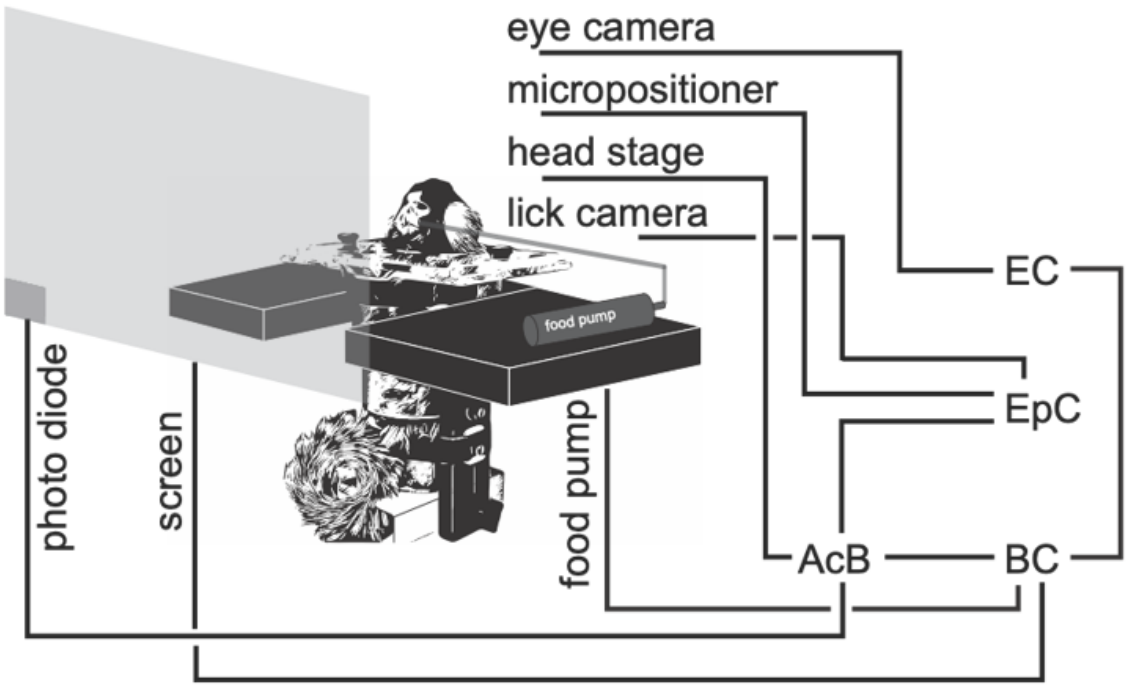

Figure 2-1. The experimental setup. AcB, EpC, BC, and EC represents the acquisition board, electrophysiological computer, behavioral computer, and eye computer, respectively. From Sedaghat-Nejad et al., 2019.

In order to record from the cerebellum, a stable subject is necessary to allow for the mobility of electrodes and longevity of recording sessions. The marmoset subjects thus required head-fixation prior

to recording. First a pre-operative CT was done of each of the marmoset subjects which was when used to create a 3D model of each subject's skull using open-source software 3D Slicer (Fedorov et al., 2012). These models were used to guide the design of each subject's custom titanium head-post, base recording chamber, and protective chamber cap. The biocompatible titanium head-post and chamber were then implanted into the subjects by a surgical team supported by veterinarians and veterinary technicians.

To plan electrode trajectories a post-operative CT was done on the subjects with a specially designed reference ruler placed in the base chamber. Registration between the pre-operative CT, pre-operative MRI, and post-operative CT provided a full representation of each subject's brain, skull, and reference ruler. This was used calculate the electrode trajectories to record from specific points in the cerebellum. The planned trajectories designed to originate from the desired recording locations, converged at the location of a burr hole and extended past the base chamber. An electrode guidance tool was designed using these trajectories and was attached to the base chamber. This tool provided a physical reference of the planned electrode trajectories and contained several cylindrical cutouts leading to the burr hole that would provide the electrodes with guidance to the desired recording locations within the cerebellum. The electrodes would be advanced into the brain using a microdrive attached to a stereotaxic micromanipulator following an alignment procedure. A craniotomy was done to create the burr hole and was sealed using a transparent silicone gel. Three types of electrodes were used to record from the subjects including quartz insulated, metal core 4 fiber tetrode and 7 fiber heptode electrodes from Thomas Recording. Additionally, 64 contact high density silicon probes from Cambridge Neurotech were also used. The open-source electrophysiology software OpenEphys (Siegle et al., 2017), was used for data acquisition purposes and interfaced with a RHD2000 communication system from Intan Technologies, USA.

During experiments the marmoset subjects were seated in an experiment chair in front of a TV screen and were tasked with making saccades to targets displayed on the TV screen. During this time, their eye movements were tracked by an EyeLink-1000 eye tracking system from SR Research, USA at 1000Hz. If a successful saccade was done by the subject a distinct auditory tone was played and a food pump was encaged that pushed food through a food tube placed just adjacent to the subject's mouth. One food tube was placed to the right of the subject and one to the left. Subjects were able to retrieve reward at their own discretion once it was within the reach of their tongues. During this time, a micropositioner along with a data acquisition system was used to drive probes to record signal from desired locations in the brain. Additionally, a photo diode was used in the experiments to measure screen delay. Finally, an overhead lick camera was used to observe and quantify licking behavior in the marmoset subjects.

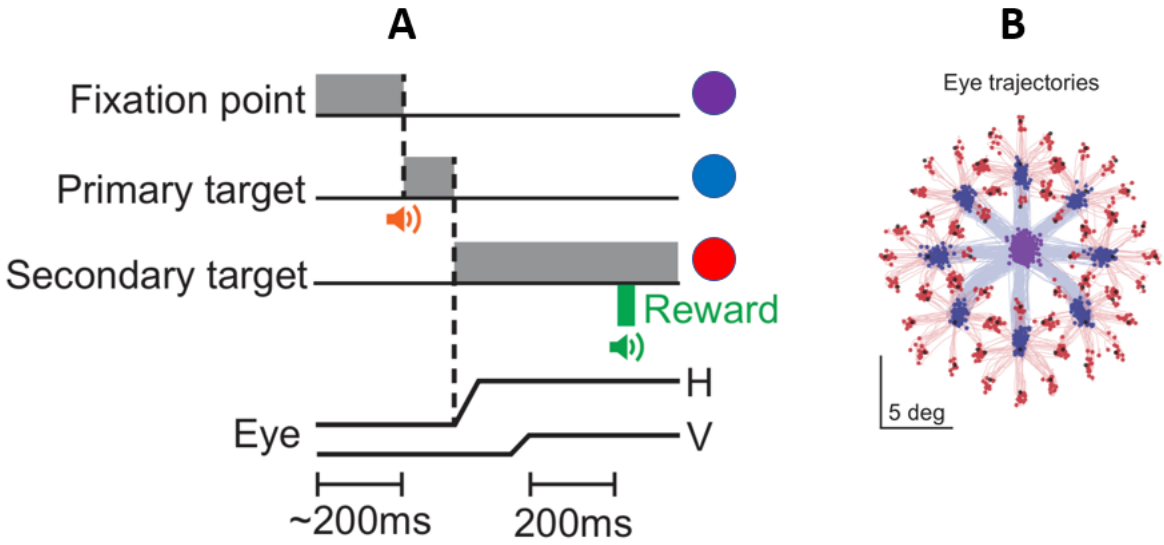

Figure 2-2. Task design and saccade results. A. Overview of task design. B. Example of recorded eye trajectories during the task. From Sedaghat-Nejad et al., 2019.

While in the experiment chair the subjects completed a task involving saccades to receive reward. The trials begin with the subjects fixated on a central target for 200ms. After this time, a primary target would appear at a random location within a distance of 5-6 degrees from the central target. As the

subject made its saccade to the primary target it was erased, and a new secondary target was generated 2-2.5 degrees from the primary target. If the subject was able to make the corrective saccade to the secondary target after making a saccade to the primary target and fixated on the secondary target for 200ms, they were given reward.

Due to the nature of the electrodes, it is possible that the recorded signal is from a number of cells and not a single Purkinje cell (P-cell). Thus, it is important to identify if the recorded signal is from a single or multiple P-cells. Since simple spikes from a single cell produce a refractory period, the probability that a simple spike occurred at a time t after a simple spike occurred at time zero, $\Pr(S(t)|S(0))$, should present a low probability during a period of 10ms centered at time zero. As simple spikes are suppressed by complex spikes, the probability that a simple spike was generated at a time t following a complex spike generated at time zero, $\Pr(S(t)|C(0))$, should indicate a long duration of low simple spike probability after time zero. By comparing the histograms of these two probabilities it could be determined that recorded complex and simple spike data was from the same cell.

2.2 Identifying Tongue Related Purkinje Cells

To identify P-cells related to lick behavior, P-cell responses were confirmed via visual and audio feedback. Specifically, it could be seen during recording that a neuron's firing rate was modulated by licking behavior. Lick related P-cells were labeled based on visual and audio feedback that indicated a significant difference in neuron firing during licking bouts versus before licking bouts. In total, 63 P-cells across lobule VI of the marmoset cerebellum were recorded and then analyzed in this paper. The recorded cells were from two marmoset subjects: subject M and subject R.

2.3 Tongue Tracking Using DeepLabCut (DLC)

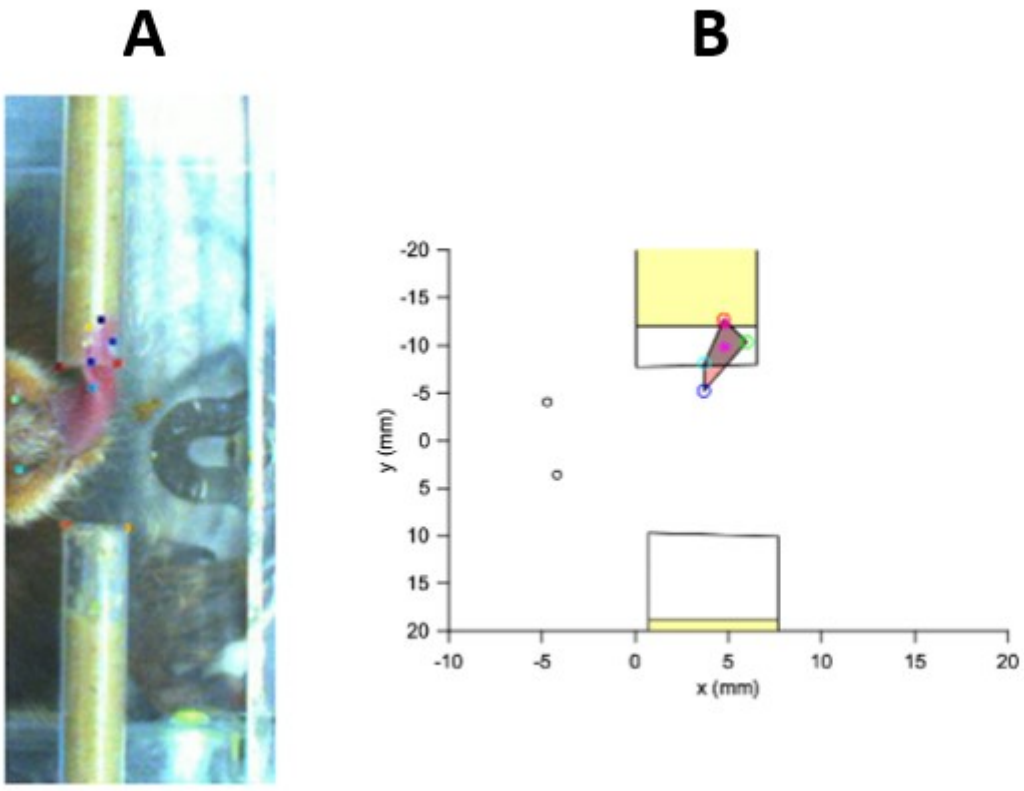

Figure 2-3. Example of tongue tracking. A. Example video frame with markerless tracking points visible. B. Example of polygon fitting to the markerless tracking data.

In order to quantify the movement of the tongue, DeepLabCut was used to perform 3D marker-less pose estimation on the tongue, food tube, and marmoset head position (Mathis et al., 2018). DeepLabCut is an open-source software that is able to execute 3D marker-less pose estimation with minimal training data through transferring learning with deep neural networks (Mathis et al., 2018). Several video frames of the lick camera recordings were labeled and were used as a training dataset for a custom network using the DeepLabCut toolbox to provide generalized tracking across lick camera videos. Markers were placed on the nostrils of the marmoset subjects, the left and right edges of the end of each food tube, the food in the tube at its most dense location, the tip of the tongue, the approximate midpoint of the

tongue, and the left and right edges of the tongue at the middle point of the length between the midpoint and the tip of the tongue. Tracking of these points allowed for the quantification of the tongue angle, velocity, and displacement away from the mouth. Fitting polygons to the markers allowed for the determinization of the outcome of the subject's licks, like whether or not the subjects retrieved reward, if the tongue missed the tube, and other outcomes. A robust quality assurance process was done to check and improve the custom network's tracking. ResNet-152 was used as the base network for the transfer learning necessary to train the custom network to track licks using the DeepLabCut toolbox (He et al., 2016).

2.4 Data Preprocessing

Given the number of sources of data used in analysis, it was paramount that all data sources be properly aligned in time in order to accurately be able to gain insight into the relationship between tongue behavior and neuron firing. The lick camera data was synchronized to the neural recordings using the LED photo diode from the experimental setup. Since the LED was visible to the lick camera, it could be used as an alignment tool as it could be seen flashing in the video and its source signal was known. Using the reference LED, dynamic time-wrapping and cross-correlation analysis was done to align the lick camera recordings with the neural data recordings. The output of the pre-processing alignment process was an alignment file used for use in post-processing. These files were created for each session.

2.5 Psort: Open-Source Cerebellar Neurophysiology Software (Sedaghat-Nejad et al., 2021)

Recording and analyzing electrophysiological data from the cerebellum and specifically Purkinje cells (P-cells) is a complex endeavor involving multiple challenges. Purkinje cells are characterized by their ability to produce both simple and complex spikes (Thach, 1967). This property makes them unique in the

cerebellum and is also what researchers can use to determine if a recorded neuron is a P-cell. Specifically, the generation of a complex spike is followed by the suppression of simple spikes (Eccles et al., 1966; Sato et al., 1992). Utilizing this property, statistical methods can be used to identify P-Cells when analyzing data recorded from the cerebellum. The open-source software Psort was used to both detect simple and complex spikes from recordings as well as to identify if the spikes were generated by the same P-cell. Psort requires user interaction to sort P-cells and is not an automated sorter. As a result, this work would not be possible without the help of Dr. Reza Shadmehr PhD., Paul Hage, and Jay Pi and their efforts in sorting recorded P-cells.

2.6 Data Postprocessing

The data corresponding to each cell analyzed in this paper was made up of data from multiple recording sessions with the subjects, however some cells were only recorded in one session. Prior to cellular level analysis, each sessions data was extracted individually and organized based on analysis needs. Data postprocessing was done in MATLAB by Mathworks, USA and involved data from alignment preprocessing, DLC kinematic analysis, and Psort output. The .psort file outputted from Psort, contained data corresponding to all of the identified simple spikes (SS) and complex spikes (CS) from the entire neurophysiological signal of the session. Since the neurophysiological data was recorded at 30,000Hz it was down sampled in post-processing to 100Hz, as data corresponding to lick camera videos were approximately recorded at 100Hz. These 100Hz spike trains were arrays the length of the recording session in time, with the number of spikes detected saved at each sample point in the array. The data file outputted by the alignment process was used to pick apart the SS and CS spike trains and align them corresponding to a particular kinematic event for each lick made by the subject in the session. These kinematic events included the onset of licking (lick onset), time of max protrusion speed (vmax), time of max retraction speed (vmin), and time at which the tongue was at its farthest point (dmax).

Corresponding to each lick, the spike train data was parsed and centered at the kinematic point of interest. The result of this process was the creation of a 2-dimensional array in which the rows corresponded to the SS or CS spike data for a single lick, 2 seconds before and 2 seconds after the kinematic point of interest. The number of rows of this array represented the number of licks analyzed from the session. In this way, it was possible to observe the nature of neuron firing at particular tongue kinematic events. Due to the large time window used to align the SS and CS spike trains to the kinematic events, the spike data for some licks had to be discarded as they occurred to close to the beginning or the end of the recording session and spike data 2 seconds before and 2 seconds after the kinematic point of interest did not exist.

The tongue kinematic data, distance of tongue tip from mouth (dtip) and velocity of tongue tip (vtip), that corresponded to the SS and CS train data was imported from the output of the DLC analysis for that specific session. Since the tongue kinematic data was sampled at a different frequency than the SS and CS trains, it was interpolated using timing data from the alignment process through the MATLAB function interp1 to also be 100Hz. Then this data was also parsed and centered at each kinematic point. The result of the process was similar to what was done to the SS and CS spike trains in that a 2-dimensional array was created in which each row corresponded to the tongue kinematic data for a single lick, 2 seconds before and 2 seconds after the kinematic point of interest.

Several 1-dimensional logical arrays were imported from the DLC analysis and used to classify licks based on their type. Licks were separated into the following types for analysis:

- The initial lick of a bout.
    - Bouts consisted of licks done in rapid succession. Marmoset rhythmic licking behavior is almost exclusively characterized by these occurrence of these bouts.
- Leftward reward-driven licks.

- Rightward reward driven licks.
- Grooming licks.
    - These are licks in which the animal does not try to retrieve reward from the food tubes, but rather licks itself to groom itself.

Using these logical arrays, it was possible to extract the specific SS and CS spike trains as well as tongue kinematic data, centered at each kinematic time point (lick onset, dmax, vmax, vmin), for each lick class. Within the data post-processing code, the SS and CS spike trains along with the tongue kinematic data (dtip and vtip), for each of the lick classes were saved for the analysis process. It is important to note that the post-processing code saved the spike trains and tongue kinematic data corresponding to the initial licks of bouts were saved with only 1 seconds before and 1 seconds after kinematic points of interest. All other data associated with the other lick classes consisted of data corresponding to 2 seconds before and 2 seconds after kinematic points of interest. Spike trains and kinematic data corresponding to the initial lick of a bout were also parsed and save based on whether bouts were leftward or rightward.

In addition to this data, different characteristics of each of the licks within a recording session were also imported from the DLC analysis output file and saved for analysis. These include the following:

- The max distance of the tip of the tongue from the mouth during licking (mm).
- The max protrusion velocity of the tip of the tongue (mm/s).
- The max retraction velocity of the tip of the tongue (mm/s).
- The inter-lick interval (ILI) of between the lick and the one after it (s).
- The instantaneous lick rate (ILR) at the time of the lick (Hz).
- The time duration of the lick (s).

Each of these characteristics were also parsed and saved occurring to the lick classifiers. ILI was calculated by taking the difference between the times of lick onset. ILR was calculated by taking the inverse of ILI (1/ILI).

Additionally, information regarding the number of licks recorded in the session, the number of licks within a bout, the duration of licking bout, and the number of bouts within a session was extracted from the DLC analysis output file and saved for analysis. Using classifiers similar to those used for individual licks, data concerning the number of licks within a bout and the duration of licking bouts was separated for leftward and rightward bouts and saved for analysis.

Given that the above post-processing process was done for each individual session, a special script was written to run the post-processing protocol for each recording session and save each individual corresponding post-processing output file. Then, a separate script was written to concatenate the data from each recording session corresponding to each cell. This script aggregated the concatenated post-processing data for each cell into a single, large output file that was used for analysis.

Chapter 3. Results

All analysis was done in MATLAB. Following the post-processing process, the singular output file containing data for each of the 63 cells was imported into an analysis pipeline script. The cross-session vertical concatenation of the 2-dimensional arrays containing the SS/CS spike data or tongue kinematic dtip/vtip data yielded large 2-D matrices in which the rows still corresponded to the SS/CS spike data or tongue kinematic dtip/vtip data for a single lick, 2 seconds before and 2 seconds after a specific lick kinematic point (lick onset, dmax, vmax, vmin). However, the number of rows now corresponded to the total number of licks across all the recording sessions of that particular cell. Matrices specific to the initial licks of bouts, leftward reward-driven licks, rightward reward driven licks, and grooming licks were all extracted from the post-processing output file. Up to this point all spike train and kinematic data for each lick from across recording sessions was conserved in these matrices. In order to gain insight into how this data looked like at a cellular level, the mean of these matrices was taken across rows. This yielded a singular row vector for each lick class. In this way, the mean of the cell neuromodulation and tongue kinematic behavior centered at each kinematic time point (lick onset, dmax, vmax, vmin) was obtained across all licks corresponding to each lick classifier (initial licks of bouts, leftward reward-driven licks, rightward reward driven licks, and grooming licks). During this step, the mean SS/CS spike trains for each cell were multiplied by 100 to yield the SS/CS firing rate. After this process was done for each cell, new matrices were constructed in which the rows corresponded to the mean SS/CS spike firing rate or tongue velocity/displacement values across licks within a cell's recording session. Separate matrices were created centered at each of the different kinematic time points (lick onset, dmax, vmax, vmin). The number rows in these matrices matched the total number of cells.

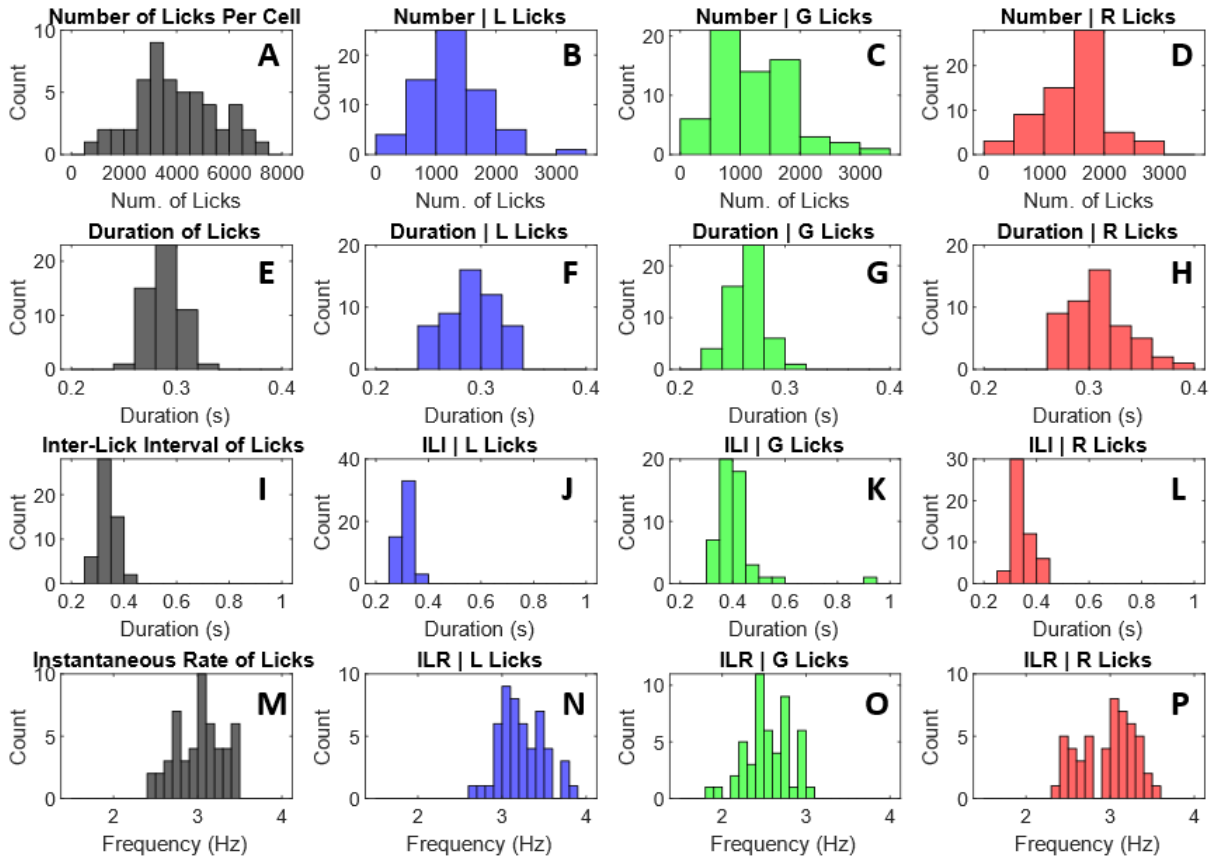

Figure 3-1. Median lick characteristics for unique recorded cells.

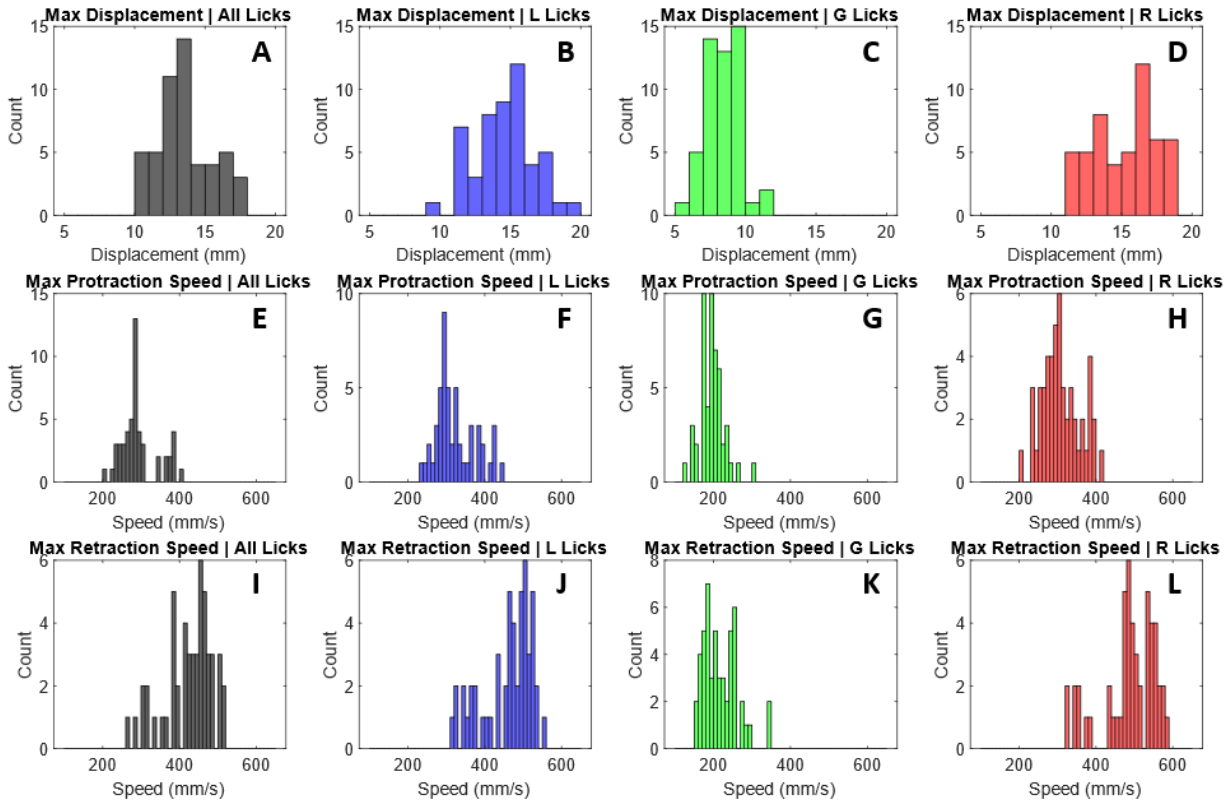

Figure 3-2. Median lick kinematic characteristics for unique recorded cells.

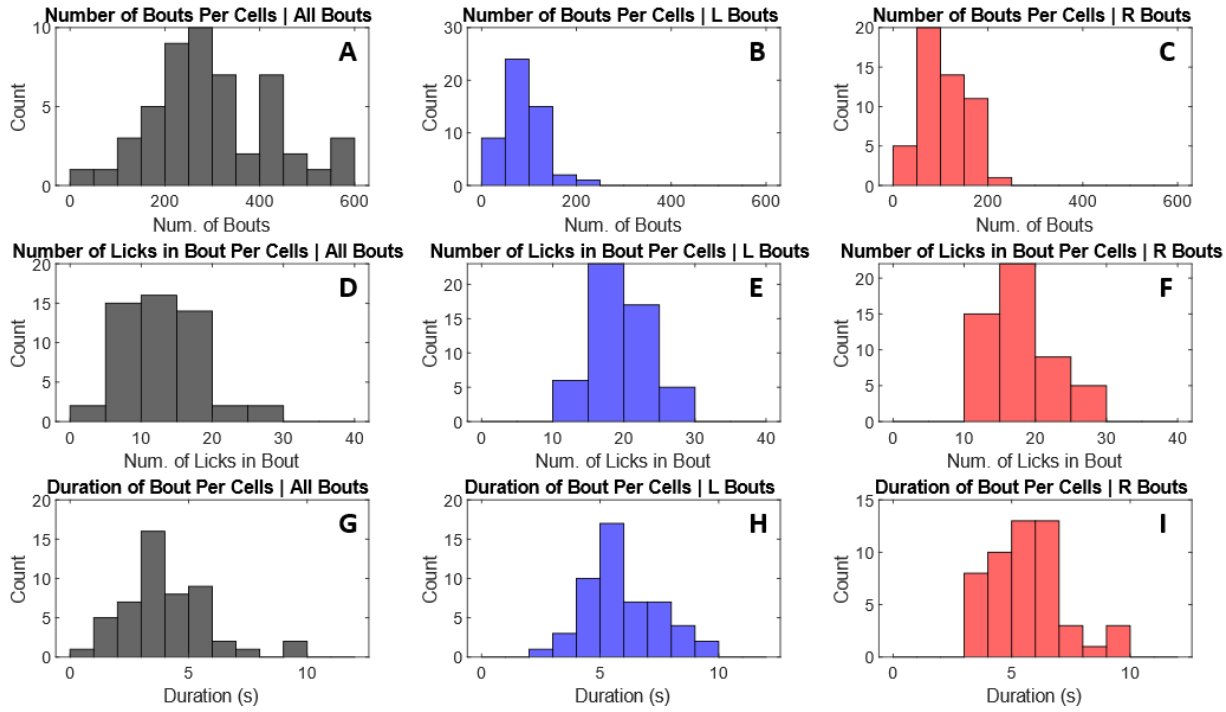

Figure 3-3. Median lick bout characteristics.

In order to examine the lick characteristic data of each lick class, that is the data regarding the max distance achieved by the tongue tip during a lick and other characteristics, at a cellular level, the median of the data across licks related to each cell was taken. A vector array with a length corresponding to the total number of cells analyzed was constructed in which each element represented the median value of a specific lick characteristic. For data concerning the number of licks within a bout and number of licking bouts recorded for each cell, the sum was taken across sessions for each cell. The histograms of these lick characteristics were provided in figures 3-1, 3-2, and 3-3. Since many of the cells were recorded simultaneously, their corresponding tongue kinematic data was the same. Given this fact, only the lick characteristics corresponding to unique tongue behavior recordings were presented in figures 3-1, 3-2, and 3-3. In total 20 cells had the same tongue kinematic data as another cell. As a result, the histograms are of median lick characteristic vector arrays 51 elements long (the number of cells with unique lick behavior recordings).

3.1 Investigating P-cell Response Properties to Lick Behavior

In order to gain insight into the response properties of P-cells to specific time points of licking behavior the following analysis was done. Cells were categorized based on a variety of factors and analyzed. Cells were grouped together based on these categories in an effort to investigate the how they fire at a population level with respect to licking. By breaking down the individual moments that make up a lick, the firing response of P-cells to these moments could also be broken down. Examining how the P-cells fire with respect to these individual lick moments could provide insight into how P-cells contribute to control of the tongue in marmosets.

3.2 Categorizing P-cells Based on their Response Properties to Lick Bouts

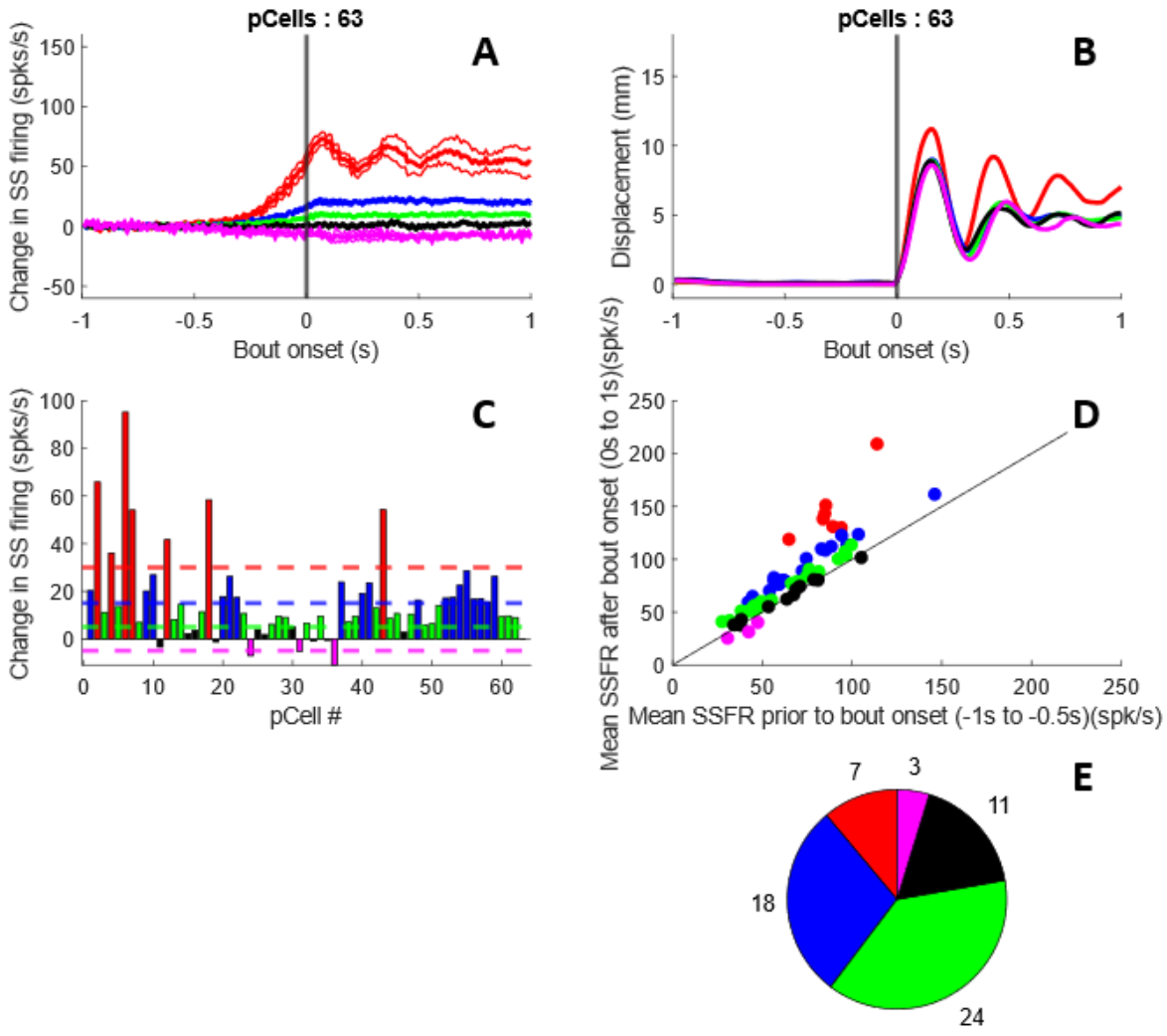

Figure 3-4. Categorizing P-cells based on their response properties to lick bouts.

The SS firing of the P-cells was first examined in response to the onset of a licking bout. The cellular SS firing rate data centered around lick onset and corresponding to the initial licks of bouts was used to accomplish this task. In order to compare the behavior of cells to each other, the mean baseline SS firing rate of each cell 1 second to 0.5 seconds prior to bout onset was subtracted from the overall cellular SS

firing rate data. This allowed for the comparison of P-cell response to bout onset by examining the change of SS firing of each cell from baseline before and after bout onset as shown in figure 3-4. The mean change of SS firing of each cell from baseline before (1s to 0.5s) and after (0s to 1s) bout onset is shown in figure 3-4C. Using a set of thresholds at 30Hz, 15Hz, 5Hz, and -5hz, the cells were labeled based on the size of their response to bout onset. Data in all plots shown in figure 3-4 were colored based on their label. Taking mean of the change in SS firing rate across cells with the same label yielded the change in SS firing traces shown in figure 3-4A. Error traces were provided using the standard error (SE) the of mean, a trace at 1 SE above the mean and a trace at 1 SE under the mean were plotted. Taking the mean of the tongue displacement kinematic data (dtip) across cells with the same label yielded the tongue displacement traces shown in figure 3-4B. To compare the SS firing rate (SSFR) before and after bout onset, the mean of each cell's SSFR trace from bout onset to 1 second afterward was taken and the mean of each cell's SSFR trace from 1 second to 0.5 seconds before bout onset was also taken. These values were plotted on Y and X axis respectively in the scatter plot shown in figure 3-4D and colored based on their label. A pie chart was created to illustrate the number of cells belonging to each label in figure 3-4E.

3.3 Categorizing P-cells Based on their Response Properties to Lick dmax

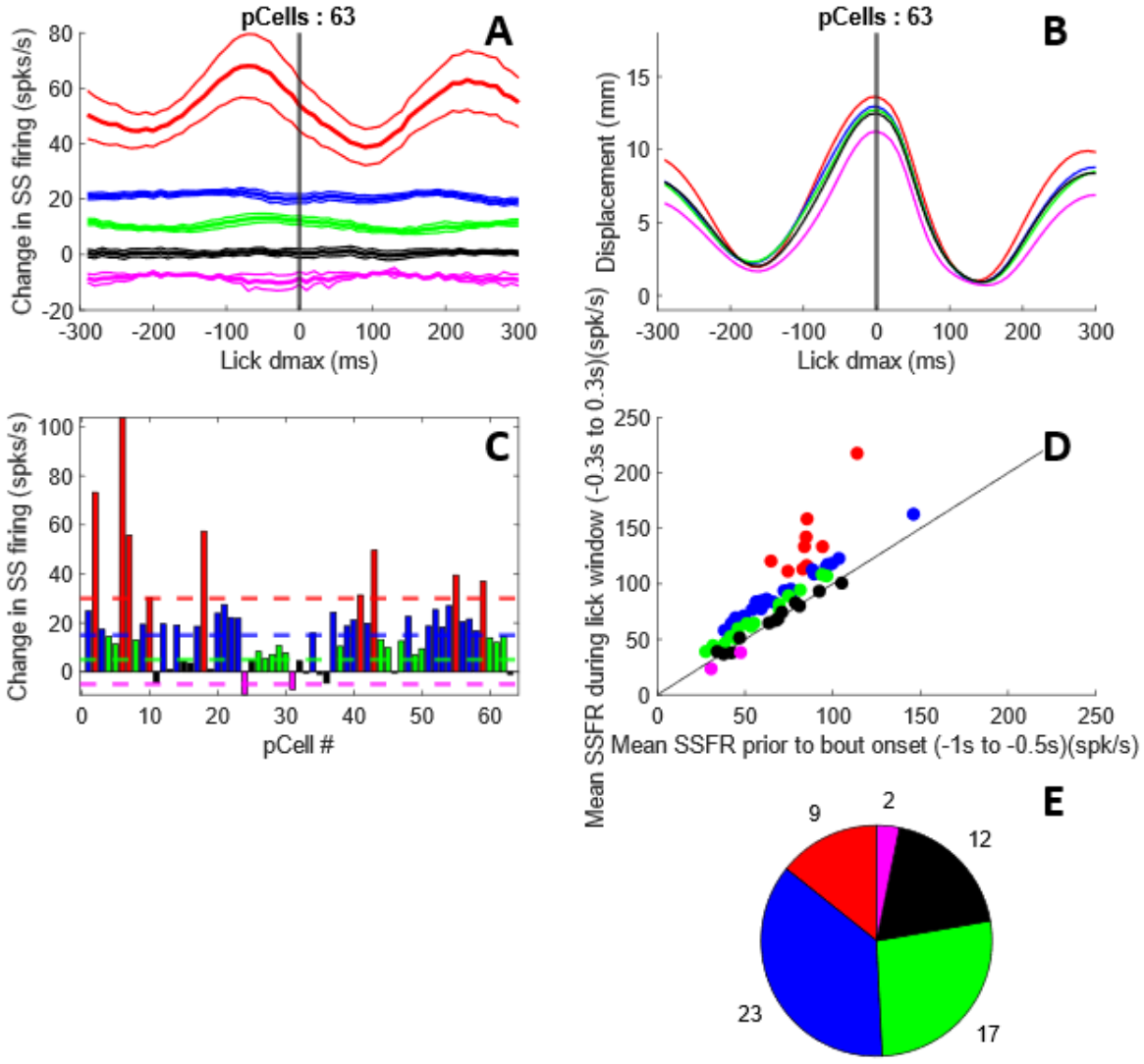

Figure 3-5. Categorizing P-cells based on their response properties to lick dmax.

The SS firing of the P-cells were then examined in response to the max displacement of the tongue from the animal's mouth (dmax). To accomplish this, the SS firing rate and tongue displacement data aligned to lick dmax of each cell was analyzed. Again, baseline firing rate was subtracted from the overall cellular SS firing rate data to allow for the comparison of the data using change in SS firing rate from

baseline. The results of this comparison were shown in figure 3-5. The mean change of SS firing of each cell from baseline before (1s to 0.5s) and around (300ms before and 300ms after) lick dmax was shown in figure 3-5C. The cells were labeled based on the size of their response to lick dmax using a set of thresholds at 30Hz, 15Hz, 5Hz, and -5hz. Taking the mean of the change in SS firing rate across cells with the same label yielded the change in SS firing traces shown in figure 3-5A. Error traces were provided using the standard error (SE) the of mean. A trace at 1 SE above the mean and a trace at 1 SE under the mean were plotted. Taking the mean of the tongue displacement kinematic data (dtip) across cells with the same label yielded the tongue displacement traces shown in figure 3-5B. To compare the P-cell responses in the time around dmax (300ms before and 300ms after lick dmax) to the baseline firing rates of each cell, the mean of each cell's SSFR trace 300ms before and 300ms after lick dmax was taken and the mean of each cell's SSFR trace from 1 second to 0.5 seconds before bout onset was also taken. These values were plotted on Y and X axis respectively in the scatter plot shown in figure 3-5D and colored based on their label. A pie chart was created to illustrate the number of cells belonging to each label in figure 3-5E.

3.4 Categorizing P-cells Based on Directional Response to Licking

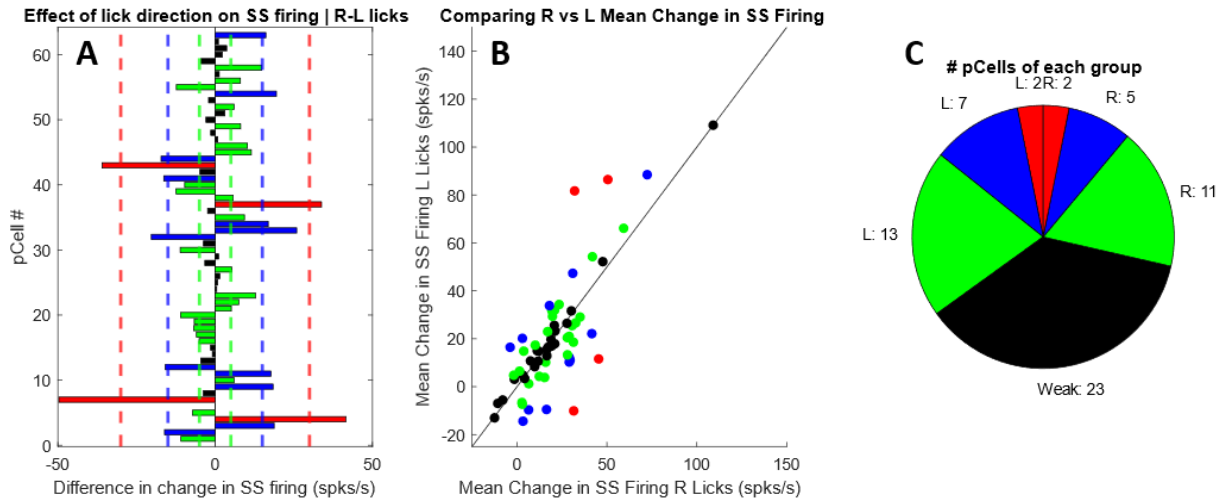

Figure 3-6. Categorizing P-cells Based on Directional Response to Licking.

Using mean change in SS firing rate data corresponding to leftward and rightward reward driven licks of each cell 300ms before and 300ms after dmax, the effect of lick direction was examined and shown in figure 3-6A. Change in SS firing was calculated by subtracting the mean baseline SS firing rate of each cell 1 second to 0.5 seconds prior to bout onset from this data. It is important to note that the value of the mean baseline SS firing rate of each cell was the same as the one used in figures 3-4 and 3-5, which used SS firing rate data corresponding to all licks to calculate the mean and was not specific to leftward and right reward driven licks. By subtracting the mean rightward lick change in SS firing data by the same data corresponding to leftward licks of each cell, it could be examined whether or not certain P-cells had a bias to firing faster in a particular direction. The mean rightward lick change in SS firing data was plotted against the mean leftward lick change in SS firing data for each cell as a scatter plot shown in figure 3-6B. Cells plotted in figure 3-6 were colored based on whether or not this difference exceeded

a 30Hz, 15Hz, or 5Hz threshold. Cells labels with a weak bias of below 5 Hz were plotted black. A pie chart was to illustrate the number of cells belonging to each group in figure 3-6C.

3.5 Identifying P-cell Responses to Licking as Non-rhythmic or Rhythmic

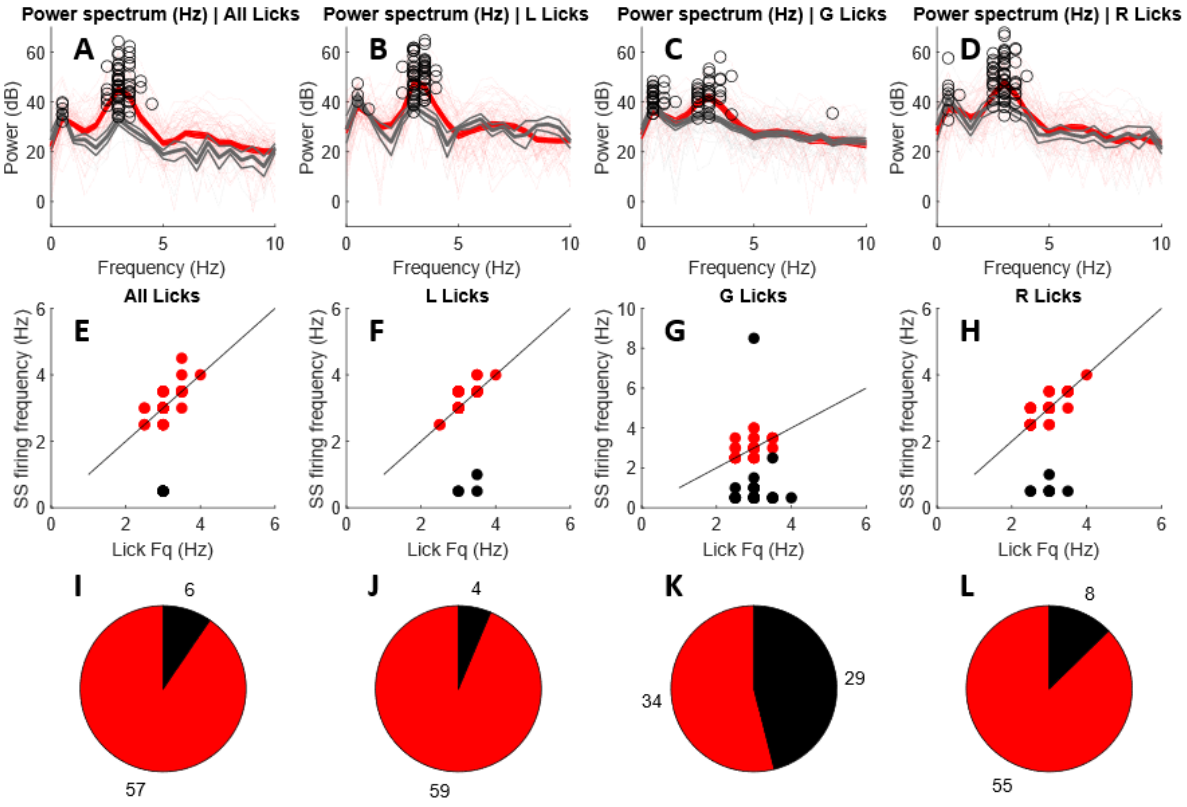

Figure 3-7. Identifying P-cell Responses to Licking as Non-rhythmic or Rhythmic.

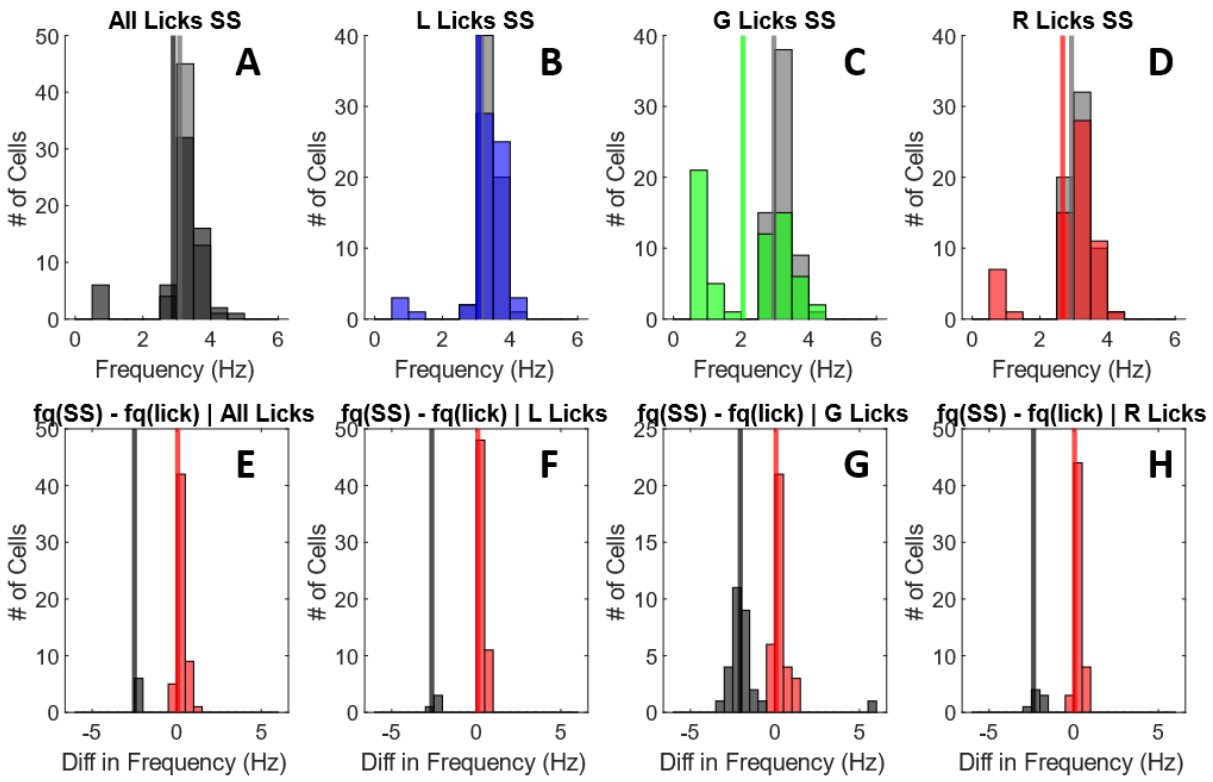

Figure 3-8. Distribution of frequencies (Hz) at max power (dB).

In order to identify P-cell responses to licking as either non-rhythmic or rhythmic, the frequency of each cell's SSFR signal was compared to that of each cell's corresponding tongue displacement waveform (dtip). Using data centered around lick dmax (1s before and 1s after), a power spectrum was generated using MATLAB's fast Fourier transform function (fft) for each signal to determine their frequencies. First the mean of each cell's SSFR or dtip signal was taken and subtracted from the original signal. This was done to remove the DC component of the signal. A high-pass filter at 0.49 Hz was applied to the signal to remove any remnants of the DC component of the signal. After this point, MATLAB's fft function was used to calculate the fast Fourier transform of the signal. The base 10 logarithm of the output of this function was multiplied by 20 to yield the power magnitude values of the signal in decibel units. This was plotted against a corresponding frequency axis to create the power spectrum of the signal. This was done for data corresponding to all licks, leftward reward-driven licks, grooming licks, and rightward

reward driven licks as seen in figures 3-7A, 3-7B, 3-7C, and 3-7D respectively. Power spectrum traces plotted in red belonged to individual cell SSFR signals and those in grey belonged to individual cell dtip signals. The mean trace of these signals was plotted with the thickest lines. Error traces were provided using the standard error (SE) the of mean, a trace at 1 SE above the mean and a trace at 1 SE under the mean. These traces were less thick, but not as transparent as the traces for individual cells. The peaks of the SSFR power spectrum for each individual cell was circled in black. The distribution of the frequency corresponding to these peaks was plotted for all licks, leftward reward-driven licks, grooming licks, and rightward reward driven licks as seen in figures 3-8A, 3-8B, 3-8C, and 3-8D respectively. The distributions related to SSFR signals were plotted in either black, blue, green, or red and the distributions related to dtip signals were plotted in gray. Vertical lines were plotted to illustrate the mean frequency of max power for both SSFR and dtip signals in their respective colors. The frequency of each cell at max power corresponding to the SSFR signals was then subtracted by the corresponding values related to dtip signals to calculate their difference in frequency. The distribution of these values was plotted for all licks, leftward licks, grooming licks, and rightward licks as seen in figures 3-8E, 3-8F, 3-8G, and 3-8H respectively. If a cell's difference in frequency was less than -0.5Hz or greater than 2Hz, it was labeled as nonrhythmic and plotted in black. If a cell did not meet these criteria, it was colored red and labeled as rhythmic. Vertical lines were plotted to illustrate the mean difference in frequency for both nonrhythmic and rhythmic cells in their respective colors. To illustrate how the frequency of peak power of both SSFR and dtip signals compare, the frequency of peak power of each cell's SSFR signal was plotted against the frequency of peak power of each cell's dtip signal for all licks, leftward licks, grooming licks, and rightward licks, as shown in the scatter plots seen in figure 3-7E, 3-7F, 3-7G, and 3-7H. Cells were colored red if labeled as rhythmic and black if labeled as non-rhythmic. Pie charts were generated to illustrate the number of cells labeled as rhythmic or nonrhythmic for all licks and lick types as can be seen in figures 3-7I, 3-7J, 3-7K, and 3-7L.

3.6 Phasic Analysis of Simple Spike Firing Rates

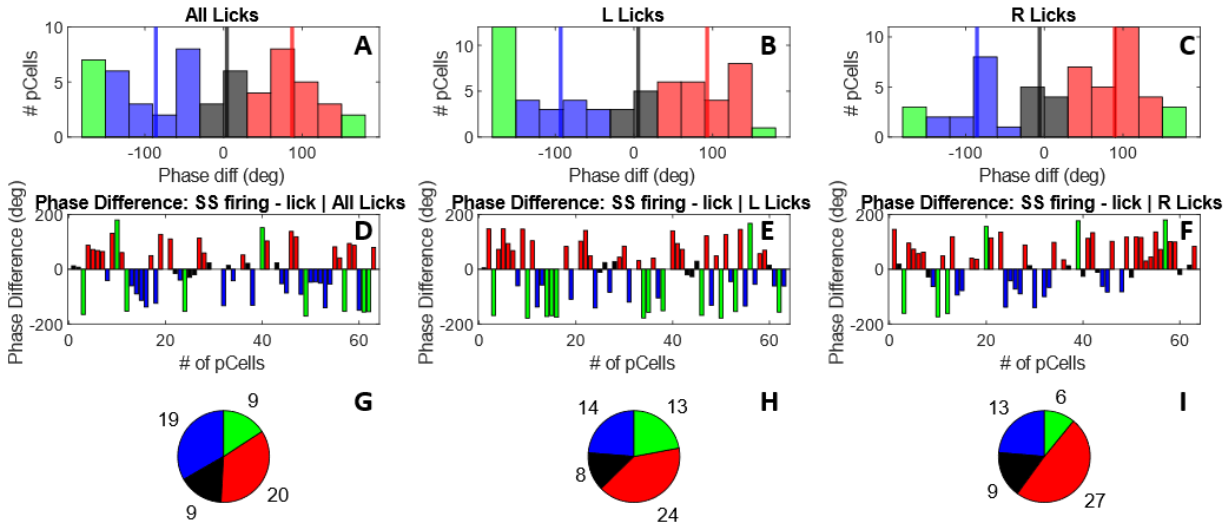

Figure 3-9. Phase difference between simple spike firing rates and tongue tip displacement.

Going forward all cells labeled as nonrhythmic were left out of analysis. In order to investigate the phasic relationship between the response of P-cells to licking, cells were categorized based on the phase difference between their SSFR signals and corresponding dtip signals. Phase difference was calculated by using a function called phdiffmeasure from MATLAB Central File Exchange (Zhivomirov, 2021). Once the phase difference was calculated for each cell, its value was plotted in bar plots shown in figure 3-9. The phase difference values concerning cell data for all licks, leftward licks, and rightward licks, were shown in figures 3-9D, 3-9E, and 3-9F, respectively. If the phase difference of a cell was calculated to be between or equal to -30 degrees and 30 degrees, it was labeled as in-phase and colored black. If a cell's phase difference was calculated to be less than -150 degrees but greater than -30 degrees, it was labeled as a lagger and colored blue. If the phase difference of a cell was greater than 30 degrees but less than 150 degrees, it was labeled as a leader and colored red. Finally, if the phase difference of a cell was greater than or equal to 150 degrees or less than or equal to -150 degrees, it was labeled as anti-phase and colored green.

The distribution of the phase difference calculated for each cell was also plotted in figure 3-9. Phase difference distributions concerning cell data for all licks, leftward licks, and rightward licks, were shown in figures 3-9A, 3-9B, and 3-9C respectively. The mean values of the phase difference distributions for in-phase, leaders, and laggers were plotted as vertical lines in their respective colors. Pie charts were included to illustrate the number of cells assigned to each group as seen in figures 3-9G, 3-9H, and 3-9I.

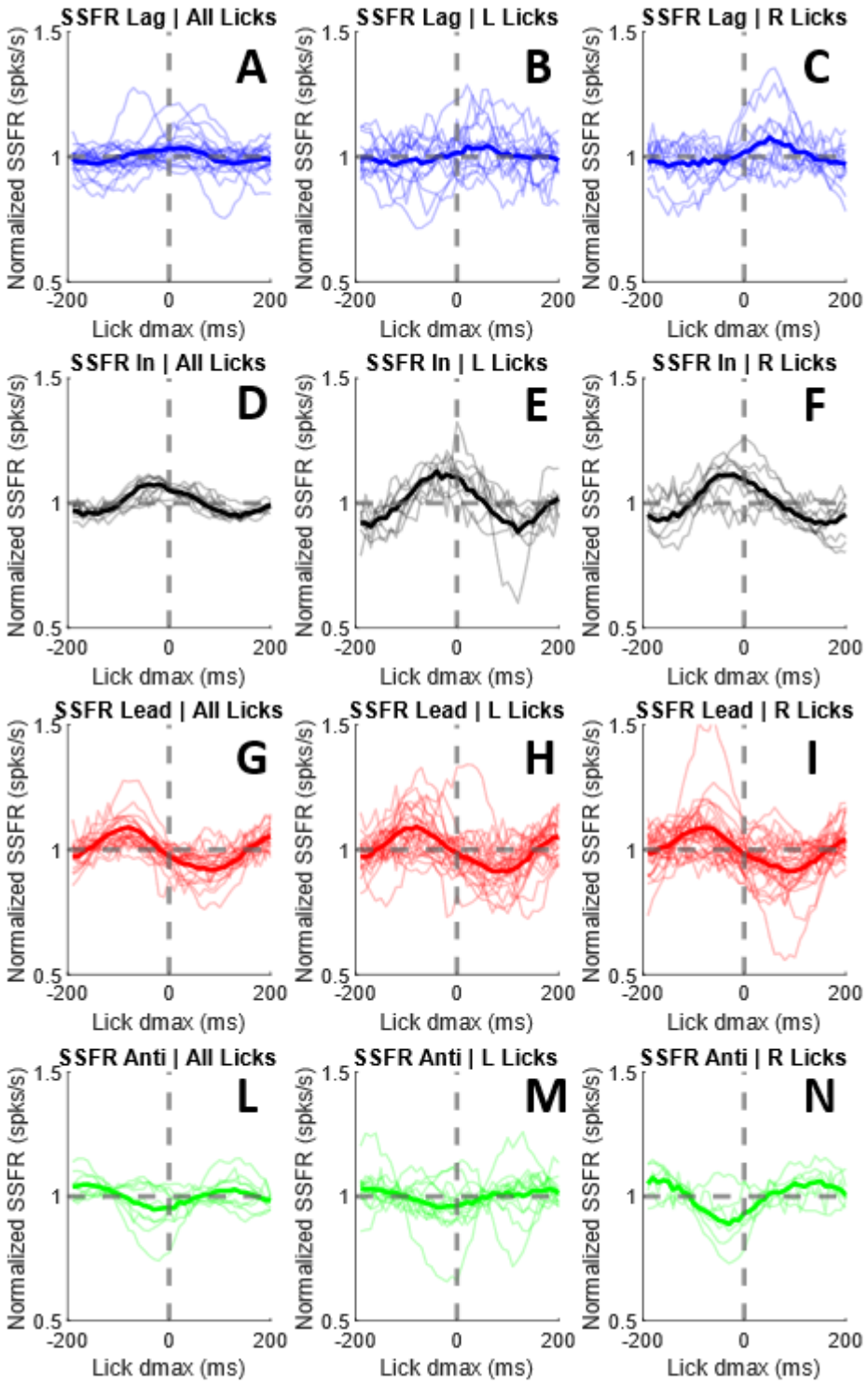

Figure 3-10. Normalized SSFR signals corresponding to cells categorized as laggers, in-phase, leaders, and anti-phase.

In order to visualize what these categories of cells look like, the SSFR signals corresponding to cells in each category were plotted as seen in figure 3-10. The signals were normalized by dividing the signal values over time by the mean of the signal values over that time period. Normalized SSFR traces of cells were illustrated in the plots as thin, semi-transparent lines. The mean trace of these cells was plotted as a thick line. Normalized SSFR traces of cells labeled as laggers were plotted for cell data corresponding to all licks, leftward licks, and rightward licks in figures 3-10A, 3-10B, and 3-10C, respectively. The same was done for the other cell categories and shown in figures 3-10D to 3-10L.

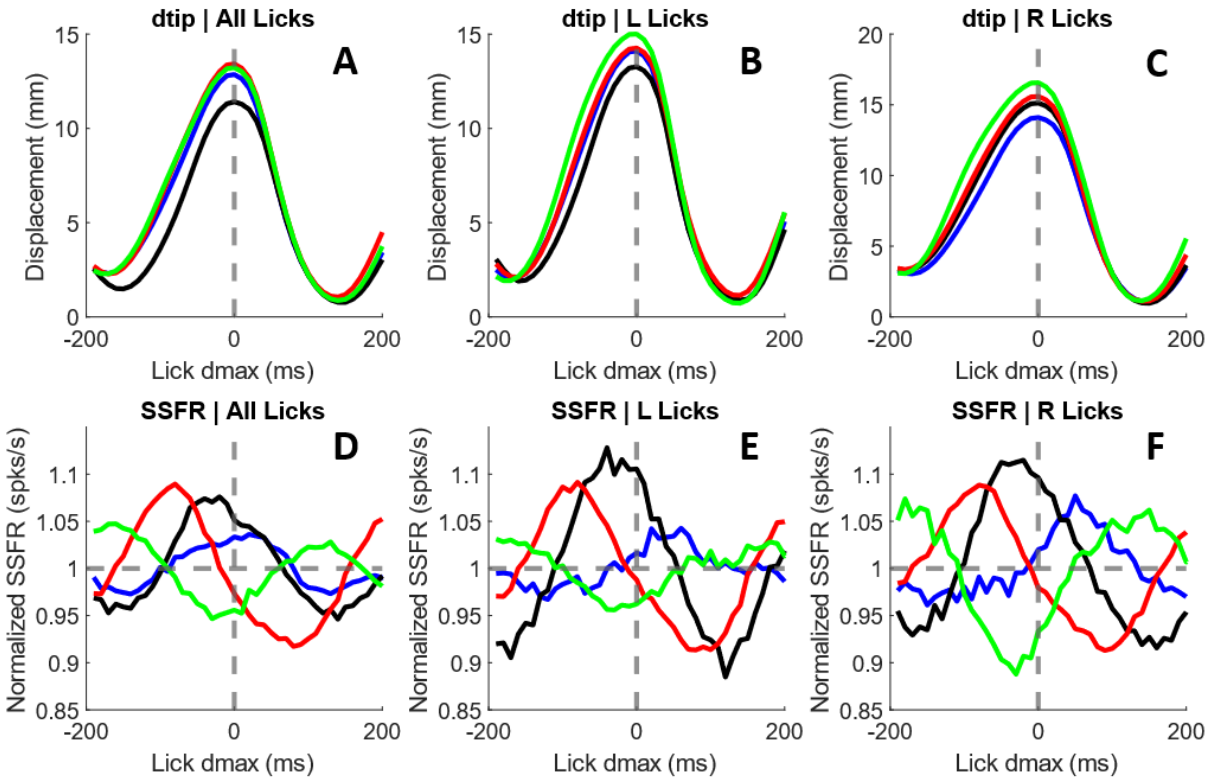

Figure 3-11. Mean normalized simple spike firing rate and tongue tip displacement of cells categorized into laggers, in-phase, leaders, and anti-phase groups overlayed with respect to max displacement of licks (dmax).

To gain a glimpse into the SS firing behavior of cells labeled as laggers, in-phase, leaders, and anti-phase at a cellular population level, the mean normalized SSFR traces shown in figure 3-10 were overlayed on top of each other and can be seen together in figure 3-11. This was done for cell data related to all licks (figure 3-11D), leftward licks (figure 3-11E), and rightward licks (figure 3-11F). In order to see the

behavior of the tongue corresponding to these groups of cells, the mean displacement signal for laggers, in-phase, leaders, and anti-phase was plotted overlapped for cell data related to all licks (figure 3-11A), leftward licks (figure 3-11B), and rightward licks (figure 3-11C).

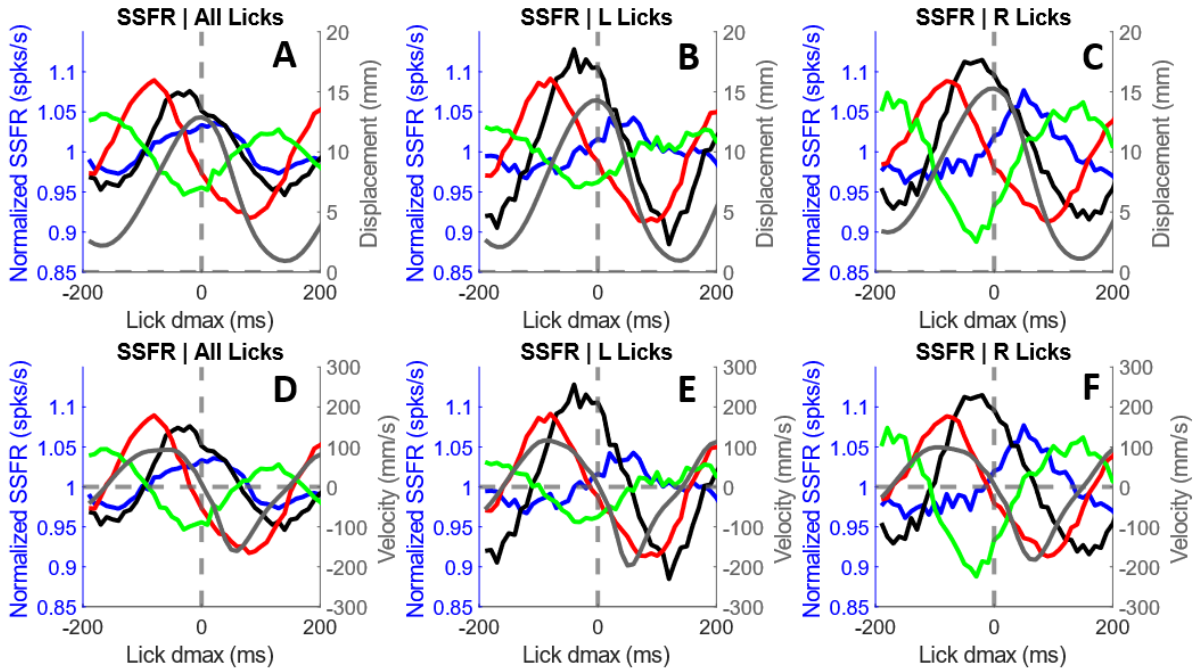

Figure 3-12. Mean tongue tip displacement and velocity of rhythmic cells overlayed with normalized SSFR of laggers, in-phase, leaders, and anti-phase groups with respect to max displacement of licks (dmax).

To better see the relationship between the mean normalized SSFR traces and the kinematics of the tongue, the same traces plotted in figures 3-11D, 3-11E, and 3-F were plotted with the mean tongue tip displacement (dtip) trace across all rhythmic cells as a shown in figures 3-12A, 3-12B, and 3-12C, respectively. The traces plotted in figures 3-11D, 3-11E, and 3-F were also plotted with the mean tongue tip velocity (vtip) trace across all rhythmic cells as a shown in figures 3-12D, 3-12E, and 3-12F, respectively. Figures 3-13 and 3-14 were created to see the same analyzed data plotted centered around the time of max tongue protraction velocity (vmax) and time of max tongue retraction velocity (vmin), respectively.

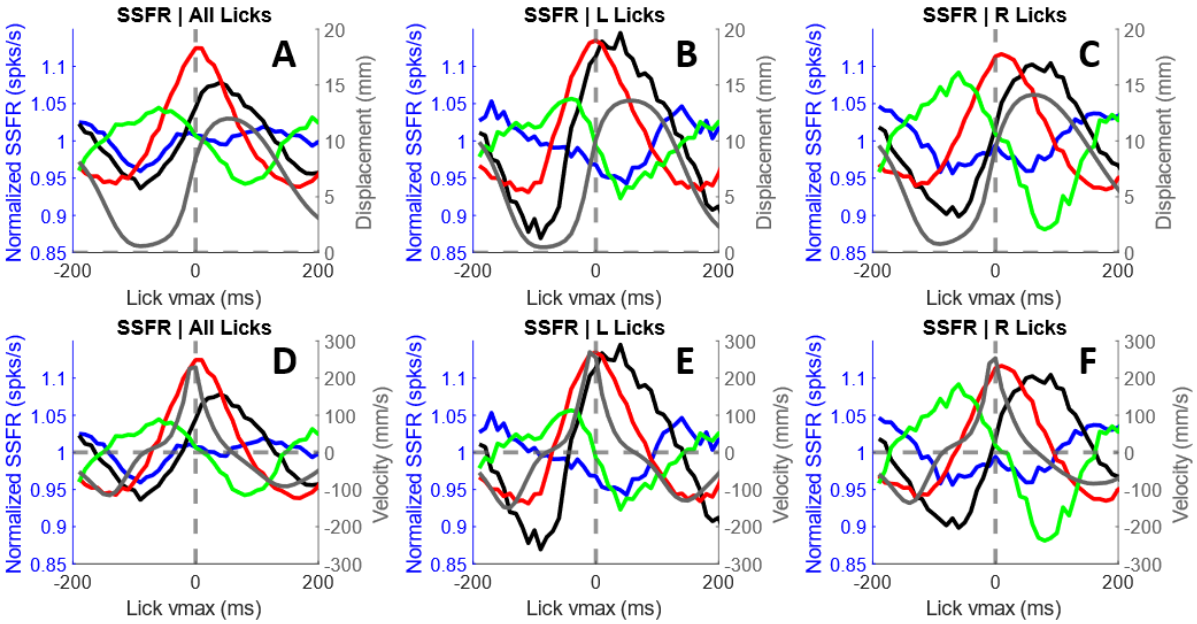

Figure 3-13. Mean tongue tip displacement and velocity of rhythmic cells overlayed with normalized SSFR of laggers, in-phase, leaders, and anti-phase groups with respect to max velocity of licks (vmax).

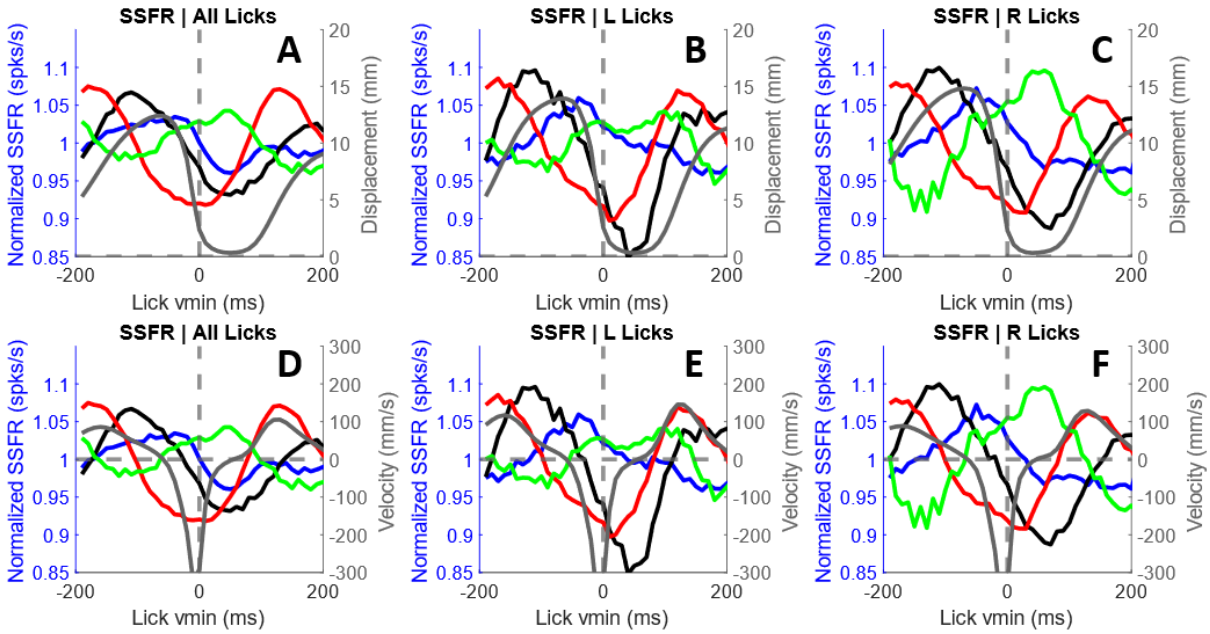

Figure 3-14. Mean tongue tip displacement and velocity of rhythmic cells overlayed with normalized SSFR of laggers, in-phase, leaders, and anti-phase groups with respect to max velocity of licks (vmin).

Chapter 4. Discussion

Examining the Purkinje cell response to the initiation of a licking bout it was observed that P-cells can exhibit a range of different firing behavior. Some cells reduce their simple spike firing rate after the onset of a licking bout, while others dramatically increase their SS firing rates. While it is unclear the reason why they behave in this way, it was apparent that some P-cells change the way they modulate in response to the onset of a licking bout whereas some continue to fire more or less at a rate similar to that of a baseline rate prior to the initiation of a licking bout. Looking at figure 3-4D, it is clear that not many cells fire at a rate lower than baseline and those that do, do not modulate as strongly as cells that fire at rate above baseline. Interestingly, reviewing the results shown in figure 3-4, it appears that cells that had a large increase (>30Hz) in SS firing rate after bout onset from baseline were associated with licks that had the largest tongue tip displacement modulation.

The P-cell response to the max displacement of the tongue tip (dmax) was of particular interest as it was the location at which the tongue, in many cases, was in contact with reward. Since the analysis done in this paper examined data from reward-driven licks and was not specific to cases in which the animal definitively retrieved reward or was unable to retrieve reward, it cannot be said that the animal definitively retrieved reward at the time of dmax. Examining the analysis done in figure 3-5 it can be seen that the extent of dtip modulation seems to correspond in order from maximum to minimum, with maximum extent achieved corresponding to cells with a large positive change in SSFR and minimum extent achieved corresponding to cells with a slightly negative change in SSFR.

Investigating the effect of lick direction on the response of P-cells to lick dmax, it could be seen that P-cells differed in their biases for leftward and rightward licks as seen in figure 3-6. The largest group of

cells consisted of those that had the weakest directional bias (sub 5Hz), however it was observed that many cells showed stronger directional bias of 15Hz or greater.

Like other animal models, the marmoset subjects exhibited rhythmic licking behavior. This could be seen in the tongue tip displacement plot shown in figure 3-4B. Observing the P-cell responses to licking, it can quickly be discerned that they appear to also fire rhythmically. To gain a better understanding of this phenomenon, the power spectrum was used on both the SSFR and dtip waveforms to extrapolate their respective frequencies. The results of this analysis showed that P-cells vary in the rhythmicity of their response to lick dmax. The distribution of these frequencies was shown in figure 3-8. It was observed that a distinct number of cells in the SSFR signal distribution were grouped at a lower frequency value than that of the other cells. It was also noted that the dtip signal distribution of the cells was grouped around the same frequency values as the majority of the data points corresponding to the SSFR signal distribution. Looking at these distributions, it was clear that some cells were firing at a frequency less than that of the marmoset's rhythmic licking. Desiring to discover the nature of P-cell rhythmic firing in response to rhythmic licks at a cellular population level, it was necessary to ignore cells that did not rhythmically fire at a rate similar to that of licking. These P-cells were labeled as nonrhythmic in analysis and not analyzed further. In general, not many P-cells were labeled as nonrhythmic as seen in figure 3-7. However, the SSFR signal for cell data corresponding to grooming licks showed a significantly higher number of cells classified as non-rhythmic for these types of licks. Moving forward, the cellular data specific to grooming licks was not examined. This was mainly due to the fact that grooming licks lacked the generalized rhythmicity seen in leftward and rightward licking.

As it was observed that P-cells vary in their rhythmic response to licking, it was also observed that rhythmic P-cells vary in their phasic relationship to lick rhythm. Calculating the phase difference between the SSFR signals and their dtip counterparts allowed for the quantification of this observation. The distribution of the phase difference values for each rhythmic cell were plotted in figure 3-9. By using

specific thresholds, the cells could be grouped as laggers, in-phase, leaders, or anti-phase based on their phase difference values and further analyzed to investigate their relationship to tongue licking behavior. Leaders were given this name due to the fact that their SSFR signals peak prior to the that of their dtip signals and this way can be said to "lead" the kinematic behavior of the tongue. The other groups of cells were also named corresponding to their relationship with tongue kinematic behavior. The SSFR signal of each cell within these groups was shown in figure 3-10. By taking the mean across the individual cell traces for each group, the laggers, in-phase, leaders, and anti-phase cells could be analyzed at a population level. These mean traces were plotted together to see how they were modulated with respect to lick dmax in figure 3-11. The corresponding mean dtip signal for these cell groups was also plotted in figure 3-11. The SSFR signal of the four groups of cells can clearly be seen as distinct, however this is not so much the case for the corresponding dtip signals of these groups. Overlaying the mean tongue tip displacement (dtip) trace and mean tongue tip velocity (vtip) trace across all rhythmic cells on top of the SSFR signal of each of these groups was done to further investigate their relationship to tongue behavior as can be seen in figures 3-12, 3-13, and 3-14. Interestingly, it was observed that in-phase P-cells appeared time-locked to the lick dmax and "lead" the signal by roughly 40ms, as seen in figure 3-12. Furthermore, it was observed that leader P-cells seem to be almost exactly time-locked to the max protraction velocity of the tongue, as seen in figure 3-13.

To conclude, it was observed that P-cells differ in their simple spike modulation from a baseline firing rate in response to the onset of licking bouts. It was also shown that P-cell simple spike firing could vary in its rhythmicity in response to rhythmic lick behavior. Examining rhythmically firing P-cells, it was observed that they can differ in their phase relationship with rhythmic licking. Cells could be classified as leading, in-phase, lagging, and anti-phase based on their phase relationship with rhythmic licking.

Moving forward it would be interesting to examine the P-cell complex spike response to licking behavior. Additionally, analysis could be done to gain insight into how the P-cell simple and complex

spike responses to licking behavior defer whether or not reward was retrieved by the animal during a lick.

Reference List

Aldes, L. D., & Bowman, J. P. (1979). Representation of the tongue in the cerebellar nuclei of the monkey. *Experimental Neurology*, *64*(1), 202–215. https://doi.org/10.1016/0014-4886(79)90015-3

Amarenco, P., & HAUW, J. J. (1990). Cerebellar infarction in the territory of the anterior and inferior cerebellar artery: a clinicopathological study of 20 cases. *Brain*, *113*(1), 139-155.

Asanuma, C., Thach, W. T., & Jones, E. G. (1983). Brainstem and spinal projections of the deep cerebellar nuclei in the monkey, with observations on the brainstem projections of the dorsal column nuclei. *Brain Research Reviews*, *5*(3), 299-322.

Barlow, S. M. (2009). Central pattern generation involved in oral and respiratory control for feeding in the term infant. *Current opinion in otolaryngology & head and neck surgery*, *17*(3), 187.

Bryant, J. (2010). Characterizing Purkinje Cell Responses and Cerebellar Influence on Fluid Licking in the Mouse. *Theses and Dissertations (ETD)*. https://doi.org/10.21007/etd.cghs.2010.0038

Bryant, J. L., Boughter, J. D., Gong, S., LeDoux, M. S., & Heck, D. H. (2010). Cerebellar cortical output encodes temporal aspects of rhythmic licking movements and is necessary for normal licking frequency. *The European Journal of Neuroscience*, *32*(1), 41–52. https://doi.org/10.1111/j.1460-9568.2010.07244.x

Byrd, K. E., & Luschei, E. S. (1980). Cerebellar ablation and mastication in the guinea pig (Cavia porcellus). *Brain Research*, *197*(2), 577–581. https://doi.org/10.1016/0006-8993(80)91150-6

Calabrese, R. L., & Marder, E. (1996). Principles of rhythmic motor pattern production. *Physiological Reviews*, *76*, 687-717.

Cifra, A., Nani, F., Sharifullina, E., & Nistri, A. (2009). A repertoire of rhythmic bursting produced by hypoglossal motoneurons in physiological and pathological conditions. *Philosophical Transactions of the Royal Society B: Biological Sciences*, *364*(1529), 2493-2500.

Cunningham, E. T., & Sawchenko, P. E. (1989). A circumscribed projection from the nucleus of the solitary tract to the nucleus ambiguus in the rat: anatomical evidence for somatostatin-28-immunoreactive interneurons subserving reflex control of esophageal motility. *Journal of Neuroscience*, *9*(5), 1668-1682.

Davis, J. D., & Smith, G. P. (1992). Analysis of the microstructure of the rhythmic tongue movements of rats ingesting maltose and sucrose solutions. *Behavioral neuroscience*, *106*(1), 217.

Downey, K. (2017, November). *Common Marmoset*. New England Primate Conservancy. https://www.neprimateconservancy.org/common-marmoset.html. Retrieved May 4, 2021.

Eccles, J. C., Llinás, R., & Sasaki, K. (1966). The excitatory synaptic action of climbing fibres on the Purkinje cells of the cerebellum. *The Journal of Physiology*, *182*(2), 268–296. https://doi.org/10.1113/jphysiol.1966.sp007824

Fedorov, A., Beichel, R., Kalpathy-Cramer, J., Finet, J., Fillion-Robin, J.-C., Pujol, S., Bauer, C., Jennings, D., Fennessy, F., Sonka, M., Buatti, J., Aylward, S., Miller, J. V., Pieper, S., & Kikinis, R. (2012). 3D Slicer as an image computing platform for the Quantitative Imaging Network. *Magnetic Resonance Imaging*, *30*(9), 1323–1341. https://doi.org/10.1016/j.mri.2012.05.001

Fujita, H., Oh-Nishi, A., Obayashi, S., & Sugihara, I. (2010). Organization of the marmoset cerebellum in three-dimensional space: Lobulation, aldolase C compartmentalization and axonal projection. *Journal of Comparative Neurology*, *518*(10), 1764–1791. https://doi.org/10.1002/cne.22301

Gordon, N. (1996). Speech, language, and the cerebellum. *International Journal of Language & Communication Disorders*, *31*(4), 359–367. https://doi.org/10.3109/13682829609031327

Halpern, B. P. (1977). Functional anatomy of the tongue and mouth of mammals. In *Drinking behavior* (pp. 1-92). Springer, Boston, MA.

He, K., Zhang, X., Ren, S., & Sun, J. (2016). Deep residual learning for image recognition. In *Proceedings of the IEEE conference on computer vision and pattern recognition* (pp. 770-778).

Hernandez-Mesa, N., Mamedov, Z., & Bureš, J. (1988). Licking during forced spout alternation in rats: resetting the pacemaker or disconnecting the motor output?. *Experimental brain research*, *70*(3), 561-568.

Hiiemae, K. M., & Crompton, A. W. (1985). Mastication, food transport and swallowing. *Functional vertebrate morphology*, 262-290.

Hooper, S. L. (2001). Central pattern generators. *e LS*.

Kim, S. Y., & Naqvi, I. A. (2020). Neuroanatomy, Cranial Nerve 12 (Hypoglossal). StatPearls Publishing, Treasure Island (FL). http://europepmc.org/books/NBK532869

Lechtenberg, R., & Gilman, S. (1978). Speech disorders in cerebellar disease. *Annals of Neurology*, *3*(4), 285–290. https://doi.org/10.1002/ana.410030402

Lin, H. C., & Barkhaus, P. E. (2009). Cranial nerve XII: the hypoglossal nerve. Seminars in neurology, 29(1), 45–52. https://doi.org/10.1055/s-0028-1124022

Marowitz, L. A., & Halpern, B. P. (1973). The effects of environmental constraints upon licking patterns. *Physiology & behavior*, *11*(2), 259-263.

Mathis, A., Mamidanna, P., Cury, K. M., Abe, T., Murthy, V. N., Mathis, M. W., & Bethge, M. (2018). DeepLabCut: markerless pose estimation of user-defined body parts with deep learning. *Nature neuroscience*, *21*(9), 1281-1289.

Nakamura, Y., & Katakura, N. (1995). Generation of masticatory rhythm in the brainstem. *Neuroscience research*, *23*(1), 1-19.

Nistri, A., Ostroumov, K., Sharifullina, E., & Taccola, G. (2006). Tuning and playing a motor rhythm: how metabotropic glutamate receptors orchestrate generation of motor patterns in the mammalian central nervous system. *The Journal of physiology*, *572*(2), 323-334.

Rangarathnam, B., Kamarunas, E., & McCullough, G. H. (2014). Role of Cerebellum in Deglutition and Deglutition Disorders. *The Cerebellum*, *13*(6), 767–776. https://doi.org/10.1007/s12311-014-0584-1

Rathee, M., & Jain, P. (2020). Anatomy, Head and Neck, Palatoglossus Muscle (Glossopalatinus, Palatoglossal). StatPearls Publishing, Treasure Island (FL). http://europepmc.org/books/NBK549823

Robbins, J., Coyle, J., Rosenbek, J., Roecker, E., & Wood, J. (1999). Differentiation of normal and abnormal airway protection during swallowing using the penetration–aspiration scale. *Dysphagia*, *14*(4), 228-232.

Sato, Y., Miura, A., Fushiki, H., & Kawasaki, T. (1992). Short-term modulation of cerebellar Purkinje cell activity after spontaneous climbing fiber input. *Journal of Neurophysiology*, *68*(6), 2051–2062. https://doi.org/10.1152/jn.1992.68.6.2051

Sedaghat-Nejad, E., Fakharian, M. A., Pi, J., Hage, P., Kojima, Y., Soetedjo, R., Ohmae, S., Medina, J. F., & Shadmehr, R. (2021). P-sort: An open-source software for cerebellar neurophysiology. *BioRxiv*, 2021.03.16.435644. https://doi.org/10.1101/2021.03.16.435644

Sedaghat-Nejad, E., Herzfeld, D. J., Hage, P., Karbasi, K., Palin, T., Wang, X., & Shadmehr, R. (2019). Behavioral training of marmosets and electrophysiological recording from the cerebellum. *Journal of Neurophysiology*, *122*(4), 1502–1517. https://doi.org/10.1152/jn.00389.2019

Siegle, J. H., López, A. C., Patel, Y. A., Abramov, K., Ohayon, S., & Voigts, J. (2017). Open Ephys: an open-source, plugin-based platform for multichannel electrophysiology. *Journal of neural engineering*, *14*(4), 045003.

Smithsonian, The National Museum of Natural History. (n.d.). Common Marmoset. Encyclopedia of Life. https://eol.org/pages/323890. Retrieved May 4, 2021.

Teune, T. M., Van der Burg, J., Van Der Moer, J., Voogd, J., & Ruigrok, T. J. H. (2000). Topography of cerebellar nuclear projections to the brain stem in the rat. In *Progress in brain research* (Vol. 124, pp. 141-172). Elsevier.

Thach, W. T. (1967). Somatosensory receptive fields of single units in cat cerebellar cortex. *Journal of Neurophysiology*, *30*(4), 675–696. https://doi.org/10.1152/jn.1967.30.4.675

Thexton, A. J. (1992). Mastication and swallowing: an overview. *British dental journal*, *173*(6), 197-206.

Travers, J. B., & Norgren, R. (1986). Electromyographic analysis of the ingestion and rejection of sapid stimuli in the rat. *Behavioral neuroscience*, *100*(4), 544.

Travers, J. B., & Rinaman, L. (2002). Identification of lingual motor control circuits using two strains of pseudorabies virus. *Neuroscience*, *115*(4), 1139-1151.

Travers, J. B., Dinardo, L. A., & Karimnamazi, H. (1997). Motor and Premotor Mechanisms of Licking. *Neuroscience & Biobehavioral Reviews*, *21*(5), 631–647. https://doi.org/10.1016/S0149-7634(96)00045-0

Vajnerová, O., Zhuravin, I. A., & Brožek, G. (2000). Functional ablation of deep cerebellar nuclei temporarily impairs learned coordination of forepaw and tongue movements. *Behavioural brain research*, *108*(2), 189-195.

Wiesenfeld, Z., Halpern, B. P., & Tapper, D. N. (1977). Licking behavior: evidence of hypoglossal oscillator. *Science*, *196*(4294), 1122-1124.

Zald, D. H., & Pardo, J. V. (1999). The functional neuroanatomy of voluntary swallowing. *Annals of Neurology: Official Journal of the American Neurological Association and the Child Neurology Society*, *46*(3), 281-286.

Zeigler, H. P. (1991). Drinking in mammals: functional morphology, orosensory modulation and motor control. In *Thirst* (pp. 241-257). Springer, London.

Zhivomirov, H. (2021). Phase Difference Measurement with Matlab (https://www.mathworks.com/matlabcentral/fileexchange/48025-phase-difference-measurement-with-matlab), MATLAB Central File Exchange. Retrieved May 4, 2021.